Persistent legacy effects on soil microbiota facilitate plant adaptive responses to drought

Nichole A. Ginnan[1,2*], Valéria Custódio[3*], David Gopaulchan[3*], Natalie Ford[1,4], Isai Salas-González[5], Dylan H. Jones[3], Darren M. Wells[3], Ângela Moreno[6], Gabriel Castrillo[3#], Maggie R. Wagner[1,4#]

[1] Kansas Biological Survey and Center for Ecological Research, University of Kansas, Lawrence, KS, USA 66045

[2] One Health Microbiome Center, Huck Institutes of the Life Sciences, Penn State University, State College, PA, USA

[3] School of Biosciences, University of Nottingham, Sutton Bonington, UK

[4] Department of Ecology and Evolutionary Biology, University of Kansas, Lawrence, KS, USA 66045

[5] Centre for Genomics Sciences. Universidad Nacional Autónoma de México

[6] Ministério da Agricultura e Ambiente, Cabo Verde

[*]These authors contributed equally

[#]Corresponding authors (gabriel.castrillo@nottingham.ac.uk and maggie.r.wagner@ku.edu)

Abstract

Both chronic and acute drought alter the composition and physiology of soil microbiota by selecting for functional traits that preserve fitness in dry conditions. Currently, little is known about how the resulting precipitation legacy effects manifest at the molecular and physiological

levels and how they influence neighboring plants, especially in the context of subsequent drought. We characterized metagenomes of six prairie soils spanning a steep precipitation gradient in Kansas, USA. By statistically controlling for variation in soil porosity and elemental profiles, we identified bacterial taxa and functional gene categories associated with precipitation. This microbial precipitation legacy persisted through a 5-month-long experimental drought and mitigated the negative physiological effects of acute drought for a wild grass species that is native to the precipitation gradient, but not for the domesticated crop species maize. In particular, microbiota with a low-precipitation legacy altered transcription of a subset of host genes that mediate transpiration and intrinsic water use efficiency during drought. Our results show how long-term exposure to water stress alters soil microbial communities with consequences for the drought responses of neighboring plants.

Introduction

The increasing frequency and intensity of droughts associated with global climate change are threatening plant health and survival in both natural and agricultural ecosystems. However, the ability of soil microbial communities to quickly adapt to environmental shifts[1] may bolster the resilience of plants and ecosystems to drought stress[2]. Additionally, the cumulative effects of past stress exposure can influence microbial communities' responses to future environmental challenges, a phenomenon referred to as legacy effects or ecological memory[3]. Despite the growing recognition of microbial legacy effects, little is known about the mechanisms driving them, their long-term persistence, and whether their effects extend uniformly across different plant species.

To investigate microbial drought legacy effects and isolate the drivers and impacts of microbial adaptations to water limitation, we (1) evaluate natural soil metagenome variation across a steep regional precipitation gradient, (2) test the ability of legacy effects to persist

through experimental perturbation, and (3) evaluate the impacts of microbiome precipitation history on plant responses to acute drought at the molecular and physiological levels. Finally, we assess the extent to which microbiome legacy effects are transferable across plant species. Our results demonstrate that legacy effects of historical exposure to dry conditions are more salient at the metatranscriptomic level than at the taxonomic or metagenomic levels, and that they trigger transcriptional changes in plant roots that improve resistance to subsequent acute droughts, at least in some plant species.

Results

Mineral nutrient accumulation and precipitation impact soil microbiota taxonomic composition

To identify microbial markers of precipitation legacy effects, we sequenced the metagenomes of soils from six never-irrigated remnant prairies spanning ~568 km of a steep precipitation gradient in Kansas, USA (Fig. 1a,b; Supplementary Table S1). Although bacterial alpha diversity was similar among soils (Extended Data Fig. 1a), community composition showed a strong biogeographic signature (PERMANOVA, R^2=0.11, p=0.001) and precipitation explained 5.3% of the variation. The first principal coordinate axis, which explained 10.6% of the total variation, separated the bacterial communities of the two highest-precipitation sites from the other soils (Fig. 1c). In line with previous findings[4], Actinomycetota and Bacillota were enriched in low-precipitation soils, whereas Pseudomonadota and Acidobacteriota were enriched in high-precipitation soils (Extended Data Fig. 1b).

To disentangle the influence of precipitation from co-varying edaphic properties[5], we examined 24 trace element profiles in each soil using ICP-MS. Nutrients are known drivers of taxonomic composition and functional capacity in soil microbiomes, particularly bacterial communities[6,7]. Mineral nutrient content differed among the six soils, with precipitation explaining 28.6% of the variation. The first principal coordinate axis of the soil mineral nutrient profiles, which explained 39.6% of the total variation, separated the three lower-precipitation sites, from the three higher-precipitation sites (Extended Data Fig. 1c). Concentrations of K, Mg, Ca, Li, and P were negatively correlated with mean annual precipitation, while Cd, Mn, Se, As, Zn, Co, Pb, Rb, Fe, and Cr were positively correlated (Extended Data Fig. 1d-e). The mineral nutrient dissimilarities among soils were correlated with the corresponding microbiota composition dissimilarities (Mantel, r=0.384; *p*-value=1e-04; Extended Data Fig. 1f). This suggests that precipitation patterns might influence the accumulation of mineral nutrients in these soils, and both precipitation and nutrients may impact microbial communities. For example, precipitation can drive mineral weathering and solute production in soils[8], although this process also depends on many other geochemical and biological factors[9].

Next, we used X-ray computed tomography to quantify soil porosity of undisturbed soil cores. Soil porosity is directly related to soil hydraulic properties; in general, lower porosity results in lower water retention and infiltration[10]. Therefore, it is a good indicator of how precipitation affects the actual water content in the soil. Consistently, soil porosity decreased with depth to about 3.5 cm before stabilizing, and increased with precipitation (Extended Data Fig. 2a-b). Notably, precipitation might affect soil porosity in surface layers of soils[11], potentially affecting soil niche properties and, consequently, microbial communities. Nevertheless, we found no correlation between the porosity dissimilarities and the microbiota composition dissimilarities of these soils (Extended Data Fig. 2c), suggesting either that soil porosity is not a key element

controlling the overall microbial community composition in these soils, or that the influence of porosity is masked by precipitation legacy.

Finally, to identify taxonomic biomarkers of precipitation legacy, we modelled the relative abundances of bacterial taxa in relation to precipitation levels while controlling for soil porosity and soil elemental composition. This analysis revealed distinct clusters of bacterial taxa whose relative abundances varied significantly along the precipitation gradient (Extended Data Fig. 2d-f). Across the six soils, 19 taxa (NCBI taxIDs) were positively correlated and nine were negatively correlated with precipitation (Fig. 1d). Additionally, 15 of the most abundant (>0.1%) and prevalent (>20%) taxa were enriched or depleted in the three lower-precipitation soils relative to the higher-precipitation soils (Fig. 1e). Together, these results indicate that water availability shapes soil bacterial communities, possibly by selecting for functions necessary to adapt to dry conditions and/or subsequent re-wetting[12].

Functional category enrichments and strain-level genetic analysis suggest molecular mechanisms of precipitation legacy effects

We used assembled metagenomic contigs to explore the functional potential of the soil communities spanning the precipitation gradient. To focus on functions that are associated with water availability rather than site-specific variation, we collapsed our six soils into two groups representing our sites with low-precipitation *vs.* high-precipitation histories. These groupings preserved the observed similarities in taxonomic composition, mineral nutrient content, and porosity (Fig. 1c; Extended Data Fig. 1c, 2a). In total, 62 Gene Ontology (GO) categories and 3396 KEGG reactions were differentially abundant between groups (Extended Data Fig. 2g; Supplementary Table S2). Biological processes enriched in low-precipitation soils included nitrogen cycling, fatty acid biosynthesis, DNA repair, and glucan metabolism, all of which have been linked to drought or stress tolerance[13–15]. Additional processes linked to stress responses

were depleted in low-precipitation soils, including ion transport (involved in osmotic adjustment), lipid catabolism (relevant for membrane integrity), and metabolism of cellular aldehydes and ketones (involved in oxidative stress)[16,17] (Extended Data Fig. 2g). The observed differences in functional potential between low-precipitation and high-precipitation sites suggest that these microbiomes are functionally adapted to local precipitation levels, making them excellent candidates for exploring how microbial precipitation legacy affects plant drought tolerance.

Next, we investigated precipitation-associated genetic variation within 33 focal bacterial species, including the previously-identified bacterial biomarkers and other highly abundant and prevalent taxa. Shotgun metagenomic reads were mapped to reference genomes from the NCBI database, and sequence variants were identified. Analysis of genetic distances showed variations in strain-level microbiome structure across the precipitation gradient (Extended Data Fig. 3a) and between precipitation levels (Extended Data Fig. 3b).

Subsequently, we conducted a genotype-environment association analysis and identified genetic variants associated with mean annual precipitation in several bacterial lineages, including *Streptomyces*, *Luteitalea*, *Rubrobacter*, *Lacibacter*, and *Rhizobium*, and three *Bradyrhizobium* lineages (Extended Data Fig. 3c, Supplementary Table S3). Most of the associated variants were located within or near protein-coding regions. Notably, some of the corresponding genes have known adaptive functions such as the phenolic acid stress response (PadR family transcriptional regulator)[18,19], maintenance of cellular functions under iron starvation and oxidative stress (Fe-S cluster assembly protein SufD and SufB)[20], and fatty acid synthesis (acetyl-CoA carboxylase biotin carboxylase subunit)[21], which impacts membrane composition and stress tolerance[17] (Extended Data Fig. 3c; Supplementary Table S3). These results indicate that precipitation legacy effects manifest through genetic differentiation within bacterial species, not just variation in community composition. Further study of these variants could reveal mechanisms by which precipitation shapes soil microbiota over ecological and evolutionary time.

Metagenomic and especially metatranscriptomic precipitation legacies are resilient to short-term perturbations

To assess the effects of short-term perturbations on soil microbiome legacy, we exposed the six focal soils to a five-month-long conditioning phase experiment. Replicate pots of each soil were either left unplanted or planted with a seedling of *Tripsacum dactyloides* (eastern gamagrass, which is native to Kansas), and were either drought-challenged or well-watered, in a factorial design (Extended Data Fig. 4a). Compared to well-watered plants, the droughted plants were shorter and had more root aerenchyma (Fig. 2a; Supplementary Fig. 4a,b), confirming that the conditioning phase drought treatment was severe enough to induce stress responses in the plants, and presumably in the microbes[22].

Next, we explored how precipitation legacy affected the microbial communities' responses to intermittent drought and watering events. Congruent with observations from the field-collected soils, water availability did not affect bacterial community alpha diversity regardless of whether a plant was present (Extended Data Fig. 4b). Although phylum-level taxonomic profiles were also similar across treatments, constrained ordination of metagenomic sequences indicated that the conditioning phase watering and host treatments explained 4.3% and 1.1% of the variation in metagenome content, respectively (Extended Data Fig. 4c-d). In contrast, precipitation legacy explained 14.1% of the metagenome variation, confirming that the conditioning phase treatments did not erase the ecological memory of these soils (Fig. 2b). Additionally, we still detected significant taxonomic differences between high- and low-precipitation soils (Supplementary Fig. 2a,b) and the previously-identified taxonomic markers of drought legacy (Supplementary Table S4) generally followed the expected enrichment and depletion patterns,

regardless of conditioning phase treatment. This resilience was particularly evident in soils with low-precipitation legacies (Fig. 2b, Supplementary Fig. 2b).

To assess whether precipitation legacy effects on strain-level genetic variation were also robust to experimental perturbation, we investigated genetic variants within the identified bacterial markers and other prevalent species across the samples, as described previously. A principal coordinate analysis of standardized pairwise genetic distances based on those variants revealed that samples clearly separated along the first axis based on precipitation legacy rather than the experimental treatments (Fig. 2c). Furthermore, our experimental perturbations did not affect allele frequencies (Supplementary Fig. 3a,b) whereas a genome-environment association analysis identified precipitation-associated genes in *Luteitalea* and two *Bradyrhizobium* lineages, recapitulating results from the pre-conditioning phase soils (Supplementary Fig. 3c, Supplementary Table S5).

Next, we tested whether functional potential still differed between low- and high-precipitation soils after 5 months of experimental perturbation. GO terms related to the nitrogen cycle metabolic process, including purine−containing compound metabolic process and pyrimidine−containing compound metabolic process, were enriched in dry-legacy soils, while GO terms related to ion transport and amino acid catabolic process were depleted in the dry-legacy soils, regardless of conditioning treatment (Supplementary Fig. 4a, Supplementary Table S6). These enrichment patterns mirrored the original field soil observations: of the 62 GO categories that were associated with precipitation legacy in the pre-conditioning soils, 49 retained the same pattern after five months of experimental drought, and 50 did so after five months of ample watering (Extended Data Fig. 2g, Supplementary Table S7). These results show that the legacy effect of precipitation on the functional capacity of soil metagenomes was robust to the conditioning phase perturbations.

Metagenome data often includes unexpressed genes and sequences from dormant or dead organisms, which could exaggerate the robustness of soil legacy effects. Therefore, we also quantified metatranscriptomes from the same samples to focus on biologically active processes across the treatments and soils. Constrained ordination showed that precipitation history explained 24.9% of the variation in microbial gene expression while conditioning phase drought and host treatments explained only 12.3% and 1.8% of the variation, respectively (Fig. 2d; Extended Data Fig. 5a). Furthermore, metatranscriptome-based taxonomic enrichment patterns confirmed the metagenome-based results: even after five months of experimental perturbation, transcriptionally active Actinomycetota and Bacillota remained enriched in low-precipitation soils while Acidobacteriota, Planctomycetota, and Pseudomonadota remained enriched in high-precipitation soils (Extended Data Fig. 5b). In general, the differences in transcriptionally active bacterial taxa between low- and high-precipitation soils mirrored our previous taxonomic-level observations, regardless of the conditioning treatments (Supplementary Fig. 2a; Extended Data Fig. 5c, 6a).

Notably, the metatranscriptome analysis revealed GO categories and KEGG reactions that remained enriched in low-precipitation soils after five months of experimental perturbation, such as tetrapyrrole metabolic process, response to osmotic stress, liposaccharide metabolic process, heme metabolic process, and trehalose catabolic process (Extended Data Fig. 6b; Supplementary Table S8-S9). These results confirm that precipitation legacy strongly shapes both functional potential and gene expression in soil microbiota, and remains robust to perturbation (*e.g.,* five-month-long acute drought). The functional resilience of the soil microbiota creates the potential for microbial legacy effects to influence host responses to environmental changes in natural ecosystems, conceivably enhancing plant resilience to future droughts.

221

222 **Microbiome precipitation legacy alters host plant responses to subsequent drought despite**
223 **taxonomic convergence of root microbiomes**

224 During the conditioning phase, we observed that droughted *T. dactyloides* plants grown in
225 low-precipitation-legacy soils were larger and produced more aerenchyma compared to plants
226 grown in high-precipitation-legacy soils (Fig. 2a). To confirm that these effects of soil
227 precipitation legacy were conferred by the microbiome rather than by co-varying soil properties,
228 we extracted the microbial communities from the conditioning phase pots and used them to
229 inoculate a new generation of *T. dactyloides* seedlings (Extended Data Fig. 4a). These "test
230 phase" plants were divided between well-watered control conditions (N=100) and a drought
231 treatment (N=200; Extended Data Fig. 4a), which we confirmed was severe enough to impair
232 plant growth (Supplementary Fig. 5a). We uprooted five-week-old gamagrass plants for
233 phenotyping and sampled crown roots, which are highly active in water acquisition[23,24], for 16S
234 rRNA gene microbiome profiling and RNA-seq analysis. We focused on bacterial microbiomes
235 because of evidence that fungi from these soils were insensitive to drought[25], and because
236 bacterial sequences accounted for 93.63% of metagenomic reads in field-collected soils and
237 89.99% in conditioning-phase soils (Supplementary Fig. 6a,b). To best capture the precipitation
238 gradient extremes, we measured gene expression only in plants inoculated with microbiota
239 derived from the two lowest-precipitation and two highest-precipitation soils.

240

241 Precipitation legacy affected neither alpha diversity nor taxonomic composition of the
242 gamagrass root microbiome (Fig. 3a). Bacterial taxonomic composition was impacted by the
243 test phase drought treatment (ANOVA.CCA, $F_{1,139}$=2.58, p=0.003) but not inoculum precipitation
244 legacy (ANOVA.CCA, $F_{1,139}$=0.89, p=0.55) (Fig. 3b); together these factors explained 2.2% of

245 root microbiome variation (ANOVA.CCA, $F_{2,139}$=1.74, R^2=0.022, p=0.01). To assess root
246 microbiome stability, we calculated beta-dispersion, a measure of within-group variability, and
247 found it to be equal among treatment groups (Fig. 3c; ANOVA, $F_{1,144}$=0.57, p=0.45). Together,
248 these results suggest that gamagrass exerts a strong homogenizing influence during root
249 microbiome formation, resulting in a stable and drought-resistant microbiota. Because eastern
250 gamagrass shares a long evolutionary history with Kansas soil microbes[26], this result supports
251 previous findings that co-evolution promotes stable community assembly[27,28].
252
253 Although precipitation legacy did not shape *16S rRNA* gene diversity within the *T. dactyloides*
254 root microbiome, its clear effect on the metagenome and metatranscriptome (Fig. 2c,d)
255 suggested high potential to influence plant phenotype. Indeed, the gene expression profiles in
256 crown roots of plants inoculated with dry-legacy microbiota were distinct from those of plants
257 inoculated with wet-legacy microbiota. Fifteen *T. dactyloides* genes were differentially expressed
258 in plants receiving a high-precipitation *vs.* low-precipitation inoculum (Fig. 4a; Supplementary
259 Table S10). Furthermore, inoculum precipitation legacy influenced the responses of 183 *T.*
260 *dactyloides* genes to acute drought (Fig. 4b). Of these, 55% were unresponsive to drought in
261 plants grown with a dry-legacy microbiota but were down-regulated or up-regulated in plants
262 grown with a wet-legacy microbiota (Fig. 4b, gene sets I and II, respectively; Supplementary
263 Table S10). This strongly suggests that soil microbiota from low-precipitation sites tend to
264 dampen the transcriptional response of gamagrass to acute drought. For instance, 50 *T.*
265 *dactyloides* genes were downregulated due to the drought treatment, but only in plants that had
266 been inoculated with high-precipitation-legacy microbiota (Fig. 4b gene set I). These included
267 five orthologs of maize genes predicted to be involved in ethylene- or ABA-mediated signalling
268 of water stress (*Td00002ba004498*, *Td00002ba024351*, *Td00002ba011993*,
269 *Td00002ba005402*, *Td00002ba000033*), and a heat shock protein linked to temperature stress
270 (*Td00002ba042486*) (Supplementary Table S10). Notably, the latter three genes were not

271 identified as drought-sensitive when averaging across inocula, demonstrating that the microbial
272 context is necessary for a complete understanding of molecular plant drought responses. We
273 note that these signatures of microbiota precipitation legacy on host gene expression are
274 averaged across all treatments applied during the conditioning phase (Extended data Fig. 4a),
275 again confirming that microbiome legacy effects are robust to short-term perturbations.
276
277 Next, we assessed whether microbial precipitation legacy altered host physiological and
278 morphological drought responses. For each of 63 traits, we calculated a drought susceptibility
279 index (S-index) that measures the stability of a trait under drought relative to control plants that
280 received the same inoculum type (Supplementary Table S11). We used a random forest model
281 to identify the ten most important traits for describing the phenotypic effects of microbiome
282 precipitation legacy (Supplementary Fig. 7a,b). Redundancy analysis revealed that microbiome
283 precipitation legacy explained 5% of the total variation in host phenotypic response to acute
284 drought (ANOVA.CCA, $F_{1,187}$=10.1, R^2=0.05, p=0.001; Extended Data Fig. 7a). Microbiota
285 precipitation legacy impacted six of the top eight non-collinear traits: transpiration, leaf
286 chlorophyll content, maximum root width, metaxylem area, median root diameter, Cu, K, and
287 intrinsic water use efficiency (iWUE)–an important plant drought response trait[29,30] (Extended
288 Data Fig. 7b-j).
289
290 To solidify the mechanisms linking microbiome legacy to plant phenotype, we used mediation
291 analysis to determine whether phenotypic drought responses were mediated by expression
292 patterns of the 198 genes that were responsive to inoculum precipitation legacy (Fig. 4a-c),
293 summarized in two dimensions (MDS1 and MDS2). MDS1 mediated 18% of the total
294 drought-induced decrease in iWUE (p < 0.001), and 8.9% of the total decrease in transpiration
295 (p=0.018; Fig. 4d). In contrast, MDS2 mediated 11% of the iWUE response to drought (p=0.03),
296 but in the opposite direction, meaning that the activity of these genes counteracted the negative

297 effects of acute drought on iWUE. Four of the top eight genes with the strongest positive
298 loadings on MDS2 were orthologs of the maize gene *ZmNAS7* (nicotianamine synthase); two of
299 these were also in the top 5% of genes with the strongest negative loadings on MDS1
300 (Extended Data Fig. 8), indicating that they stabilize iWUE during drought. All four *ZmNAS7*
301 orthologs were up-regulated in response to drought, but only in plants that were inoculated with
302 dry-legacy microbiota (Fig. 4b, gene set IV), suggesting a possible mechanism by which
303 low-precipitation-legacy microbiota confer drought tolerance. Consistent with this, salicylic
304 acid–a key regulator of root microbiome assembly[31]–is reported to induce expression of
305 *ZmNAS7*[32]. Although nicotianamine is best known for its role in metal transport, the
306 overexpression of *NAS* genes has conferred drought tolerance, including maintenance of
307 photochemical efficiency at pre-drought levels, in rice[33] and in the grass *Lolium perenne*[34].
308 Together, these results show that microbiomes with a low-precipitation legacy improve the
309 drought response of eastern gamagrass.
310

311 **Beneficial microbiome legacy effects do not extend to the crop species *Zea mays***

312 To explore whether the observed microbial legacy effects were transferable across hosts, we
313 simultaneously applied the same inocula to seedlings of maize (*Zea mays* ssp. *mays*), a relative
314 of eastern gamagrass that is non-native to Kansas (Extended Data Fig. 4a). Unlike eastern
315 gamagrass, the maize root microbiome retained taxonomic signatures of both the inoculum
316 precipitation legacy (Fig. 3e., ANOVA.CCA, $F_{1,255}$=4.25, p=0.001) and the drought treatment
317 (ANOVA.CCA, $F_{1,255}$=8.06, p=0.001) (Fig. 3e), which together explained 4.1% of the variation in
318 the data (ANOVA.CCA, $F_{2,255}$=6.16, R^2=0.041, p=0.001). Also unlike in gamagrass, drought
319 treatment significantly increased beta-dispersion and decreased alpha diversity (Fig. 3d,f;
320 ANOVA $F_{1,262=}$18.17, p<0.001), indicating lower microbiome stability.
321

322 Next, we identified amplicon sequence variants (ASVs) that were differentially abundant
323 between droughted *vs.* control plants in a manner that depended on the precipitation legacy of
324 the inoculum. These included only two ASVs in gamagrass roots (*Azospirillum* sp. and
325 *Enterobacteriaceae*), but 100 ASVs in maize roots (Supplementary Fig. 8a-b, Supplementary
326 Table S12). Again, this result indicates that gamagrass root microbiomes are more stable–*i.e.*,
327 they experience less change in microbiome taxonomic composition and assembly–than those of
328 maize, in response to varying water availability and inoculation with different starting
329 communities.
330
331 RNA-seq analysis identified four sets of orthologous genes that were sensitive to microbiota
332 legacy in both maize and gamagrass, but none showed congruent drought responses
333 (Supplementary Note 1). In maize, 23 genes were up-regulated plants inoculated with
334 dry-legacy microbiota, relative to those that received wet-legacy inocula (Extended Data Fig.
335 9a). These included six defense-related genes, particularly related to jasmonic acid signalling,
336 suggesting that low-precipitation-legacy microbiota were perceived as pathogens by maize but
337 not gamagrass. Other notable functions that were up-regulated by the dry-legacy inocula
338 include root development and iron acquisition (Supplementary Table S10). Additionally, 109
339 maize genes responded to drought treatment in a manner that was dependent on inoculum
340 precipitation legacy. Only 30 of these were identified as drought-responsive when averaging
341 across inocula (Extended Data Fig. 9b), reinforcing the importance of microbial context for
342 understanding plant drought responses. Like in gamagrass, most of these genes were
343 drought-responsive only in wet-legacy-inoculated or only in dry-legacy-inoculated plants;
344 relatively few reversed the direction of their drought response (Extended Data Fig. 9c). For
345 example, 30 genes were up-regulated in response to drought only in plants grown with
346 wet-legacy microbiota (Extended Data Fig. 9c, gene set I). These genes included several
347 related to pathogen defense (*Zm00001eb116230*, *Zm00001eb150050*, *Zm00001eb222540*) and

348 response to symbiotic fungi (*Zm00001eb033580*), suggesting that soils in high-precipitation
349 regions contain both harmful and beneficial microorganisms and that interactions with both
350 groups are activated under water deprivation in maize (Supplementary Table S10). Notably, one
351 of the genes that reversed its drought response depending on the inoculum's precipitation
352 legacy was *TIP3*, which encodes an aquaporin that regulates water storage in the vacuole[35]. In
353 plants inoculated with wet-legacy microbiota, *TIP3* expression increased 7-fold due to drought,
354 but decreased nearly 3-fold in plants inoculated with dry-legacy microbiota (Extended Data Fig.
355 9c, gene set VI). Averaged across the two inocula, however, *TIP3* was not differentially
356 expressed between droughted and well-watered plants; thus, its role in drought response was
357 apparent only when accounting for microbiota precipitation legacy.
358
359 Finally, we investigated whether the beneficial effects of microbiome legacy on gamagrass
360 phenotype (Fig. 4d-e) were also conferred on maize. Overall, microbiome precipitation legacy
361 explained only 2.0% of the phenotypic variation in maize (Extended Data Fig. 15a.,
362 ANOVA.CCA, $F_{1,175}$=3.72, R^2=0.02, p=0.001), a weaker effect than observed in eastern
363 gamagrass. In general, we observed no significant phenotypic differences attributable to
364 microbiome legacy (Extended Data Fig. 10b,c). Thus, the capacity to integrate the beneficial
365 effect of soil drought legacy is host-specific and may be related to the ability of the host to
366 maintain a stable microbiota in response to drought stress.

367 Discussion

368 Microbially-mediated legacy effects of water limitation can affect plant performance during
369 subsequent droughts[36,37]. Our results reveal how these legacy effects manifest in terms of
370 microbiota taxonomic composition, functional potential, gene expression, and strain-level
371 genetic variation, and how they affect host responses to water-scarce conditions. We identified

372 bacterial taxa and numerous microbial genes and functional pathways that are associated with
373 mean annual precipitation, including those suggesting an increased nitrogen-metabolizing and
374 DNA repair capacity in dry-legacy microbiota. Thus, we provide evidence for the ecological and
375 molecular mechanisms involved in the formation of soil drought memory and demonstrate its
376 robustness to a five-month perturbation, which could mimic a particularly dry or wet season.
377
378 We have shown that these metagenomic precipitation legacies have significant implications for
379 plant response to drought. Inoculation with dry-legacy microbiota altered the transcription of key
380 genes controlling plant drought responses. In the prairie grass *Tripsacum dactyloides*, dry- and
381 wet-legacy soil microbiomes give rise to taxonomically similar root bacterial communities yet
382 have strikingly different effects on plant gene expression and phenotypes during a subsequent
383 acute drought. These benefits largely did not extend to maize, which also had a relatively
384 unstable root microbiome and reduced physiological and morphological sensitivity to soil
385 microbiome legacy during drought. However, further research is needed to confirm whether root
386 microbiome stability is a mechanism of adaptive plant responses to drought. Importantly,
387 differences between gamagrass and maize responses to microbiome history indicate that crops
388 may not reap the same benefits as native plant species from potentially beneficial microbial
389 communities. Therefore, our discoveries significantly contribute to our mechanistic
390 understanding of microbiome drought legacy effects, their resistance to perturbation, and their
391 role in plant drought responses, with implications for agricultural and ecosystem management.

392 Online Methods

393 No statistical methods were applied to predetermine sample size. The experiments were
394 randomized, and investigators were blinded to allocation during experiments and outcome
395 assessment.

1. Legacy phase: Characterization of soils across precipitation gradients

1.1 Region selection and soil collection

Soils were sampled from six never-irrigated native prairies across Kansas, USA in October 2020. This selection includes eastern Kansas tallgrass prairies: Welda Prairie (WEL), Clinton Wildlife Reserve (CWR), and Konza Wildlife Reserve (KNZ), as well as western Kansas shortgrass prairies: Hays Prairie (HAY), Smoky Valley Ranch (SVR), and Kansas State University's Tribune Southwest Research Center (TRI). The GPS coordinates of each collection site are available in the Supplemental Table S1. For soil collection, each site was split into three subplots. In each subplot, the surface soil (≈10 cm) containing thick plant root masses was removed with a bleach-sterilized metal shovel. Then, approximately 2.5 L of soil was collected from each site and pooled into a clean plastic bag, for a total of ≈7.5 L of soil collected per geographical location. Soil was held at room temperature for transport back to the laboratory where it was then stored at 4˚C until use in the growth chamber experiments (~ 1 month).

Sub-samples for downstream metagenomic sequencing and nutrient mineral content analyses were air-dried in sterile plastic trays at room temperature for 1 week and then sieved using a 2 mm sieve to remove rocks, big soil particles, and vegetable debris. The sub-samples were shipped to the University of Nottingham for further processing, and all sub-samples were stored at 4 ºC until use (~3 days).

1.2 Precipitation data collection

Daily precipitation from 1981 to 2021 was extracted from the NASA POWER database based on the latitude and longitude of each site[38].

420 *1.3 Soil elemental content analysis*

421 The soil mineral nutrients and trace elements profiles were determined using inductively
422 coupled plasma mass spectrometry (ICP-MS). The soil samples were dried using plastic
423 weighing boats in the fume hood for approximately 72 h at ambient temperature. Five grams of
424 soil were weighed in 50 mL conical tubes with a four-decimal balance, and treated with 20 mL of
425 1 M NH_4HCO_3, 5 mM diamine-triamine-penta-acetic acid (DTPA), and 5 mL 18.2 MΩcm Milli-Q
426 Direct water (Merck Millipore), for 1 h at 150 r.p.m. in a rotary shaker (adapted from[39]) to extract
427 available elements. Each treated sample was gravity-filtered through a quantitative filter paper
428 (Whatman 42- WHA1442070) to obtain approximately 5 mL of filtrate. Prior to the digestion, 20
429 µg/L of Indium (In) was added to the nitric acid Primar Plus (Fisher Chemicals) as an internal
430 standard for assessing error in dilution, variations in sample introduction and plasma stability in
431 the ICP-MS instrument. Next, 0.5 mL of the soil filtrates were open-air digested in glass Pyrex
432 tubes using 1 mL of concentrated trace metal grade nitric acid spiked indium internal standard
433 for 2 h at 115 ºC in dry block heater (DigiPREP MS, SCP Science; QMX Laboratories, Essex,
434 UK). After cooling, the digests were diluted to 10 mL with 18.2 MΩcm Milli-Q Direct water and
435 elemental analysis was performed using an ICP-MS, PerkinElmer NexION 2000 equipped with
436 Elemental Scientific Inc 4DXX FAST Dual Rinse autosampler, FAST valve and peristaltic pump.
437 The instrument was fitted with PFA-ST3 MicroFlow nebulizer, baffled cyclonic C3 high sensitivity
438 glass spray chamber cooled to 2ºC with PC3X Peltier heated/cooled inlet system, 2.0 mm i.d.
439 quartz injector torch and a set of nickel cones. Twenty-three elements were monitored including
440 following stable isotopes: ^{7}Li, ^{11}B, ^{23}Na, ^{24}Mg, ^{31}P, ^{34}S, ^{39}K, ^{43}Ca, ^{52}Cr, ^{55}Mn, ^{56}Fe, ^{59}Co, ^{60}Ni, ^{63}Cu,
441 ^{66}Zn, ^{75}As, ^{82}Se, ^{85}Rb, ^{88}Sr, ^{98}Mo, ^{111}Cd, ^{208}Pb and ^{115}In. Helium was used as a collision gas in
442 Kinetic Energy Discrimination mode (KED) at a flow rate of 4.5 mL/min while measuring Na, Mg,
443 P, S, K, Ca, Cr, Mn, Fe, Ni, Cu, Zn, As, Se and Pb to exclude possible polyatomic interferences.
444 The remaining elements were measured in the standard mode. Any isobaric interferences were
445 automatically corrected by the instrument Syngistix™ software for ICP-MS v.2.3 (Perkin Elmer).

446 The ICP-MS measurements were performed in peak hopping scan mode with dwell times
447 ranging from 25 to 50 ms depending on the element, 20 sweeps per reading and three
448 replicates. The ICP-MS conditions were as follows: RF power – 1600 Watts, auxiliary gas flow
449 rate 1.20 L/min. Torch alignment, nebulizer gas flow and quadrupole ion deflector (QID) voltages
450 (in standard and KED mode) were optimized before analysis for highest intensities and lowest
451 interferences (oxides and doubly charged ions levels lower than 2.5%) with NexION Setup
452 Solution containing 1 µg/L of Be, Ce, Fe, In, Li, Mg, Pb and U in 1% nitric acid using a standard
453 built-in software procedure. To correct for variation between and within ICP-MS analysis runs,
454 liquid reference material was prepared using pooled digested samples, and run after the
455 instrument calibration, and then after every nine samples in all ICP-MS sample sets. Equipment
456 calibration was performed at the beginning of each analytical run using seven multi-element
457 calibration standards (containing 2 µg/L In internal standard) prepared by diluting 1000 mg/L
458 single element standards solutions (Inorganic Ventures; Essex Scientific Laboratory Supplies
459 Ltd) with 10% nitric acid. As a calibration blank, 10% nitric acid containing 2 µg/L In internal
460 standard was used and it was run throughout the course of the analysis.
461
462 Sample concentrations were calculated using the external calibration method within the
463 instrument software. Further data processing, including the calculation of final elements
464 concentrations was performed in Microsoft Excel. First, sample sets run at different times were
465 connected as an extension of the single-run drift correction. Linear interpolation between each
466 pair of liquid reference material standards was used to generate a theoretical standard for each
467 sample that was then used to correct the drift by simple proportion to the first liquid reference
468 material standard analysed in the first run. Liquid reference material composed of pooled
469 samples was used instead of the CRM to match the chemical matrix of the samples as closely
470 as possible, thereby emulating the sample drift. Second, the blank concentrations were
471 subtracted from the sample concentrations and each final element concentration was obtained

472 by multiplying by the dilution factor and normalizing the element concentrations to the sample's
473 dry weight.
474

475 *1.4 Soil porosity analysis*

476 To quantify soil porosity, we used X-ray computed tomography. First, six soil samples were
477 collected in October 2020 from each of the selected locations in Kansas (see materials and
478 methods 1.1). The top layer of soil was removed (10 cm), and the soil samples were collected
479 using polyvinylchloride (PVC) columns of 5 cm internal diameter and 7 cm length. After the soil
480 collection, the bottom of each column was sealed with tape to retain the soil in the column.
481

482 The undisturbed soil columns were non-destructively imaged using Phoenix v|tome|x MDT
483 (Waygate Technologies GmbH, Wunstorf, Germany) at The Hounsfield Facility, University of
484 Nottingham. Scans were acquired by collecting 2695 projection images at 180 kV X-ray energy,
485 200 µA current and 334 ms detector exposure time in fast mode (15 min total scan time per
486 column). Scan resolution was 55 µm.
487

488 *1.5 Metagenomic analysis of free-living soil microbiota - DNA extraction*

489 For metagenomic analysis, approximately 5 g of each soil sample was transferred into 50-mL
490 conical tubes containing 20 mL of sterile distilled water. To remove large plant debris and soil
491 particles, the samples were shaken thoroughly and filtered into new sterile 50-mL tubes using
492 100-µm nylon mesh cell strainers. The filtered soil solutions were centrifuged at high speed for
493 20 min in a centrifuge Eppendorf 5810R and most of the supernatants were discarded. The
494 remaining 1-2 mL of supernatants were used to dissolve the soil pellets. The resulting
495 suspensions were transferred to sterile 1.5-mL Eppendorf tubes. Samples were centrifuged
496 again at high speed in a benchtop centrifuge and the supernatants were discarded. The

497 remaining pellets were stored at - 80ºC for DNA extraction. For DNA isolation we used
498 96-well-format MoBio PowerSoil Kit (MOBIO Laboratories; QIAGEN) following the
499 manufacturer's instructions. Before starting the extraction, all samples were manually
500 randomized by placing them in a plastic bag that was shaken several times. Samples were then
501 taken individually from the bag and loaded in the DNA extraction plates. This random
502 distribution was maintained throughout library preparation and sequencing.
503

504 *1.6 Metagenomic library preparation and sequencing*

505 DNA sequencing libraries were prepared using the Rapid PCR Barcoding Kit (SQK-RPB004)
506 from Oxford Nanopore Technologies, UK. In brief, 1 µL Fragmentation Mix (FRM) was added to
507 3 µL DNA (2-10 ng/µL), and the reaction was mixed by gently finger-flicking. The DNA was
508 fragmented using the following conditions: 30°C for 1 min, then 80°C for 1 min in an Applied
509 Biosystems Veriti 96-Well Thermal Cycler (Applied Biosystems, CA, USA). The fragmented DNA
510 was cooled, then barcoded and amplified in a PCR reaction containing 20 µL nuclease-free
511 water, 25 µL LongAmp Taq 2X master mix (New England Biolabs, MA, USA), 4 µL fragmented
512 DNA, and 1 µL barcode adaptor. The reaction was gently mixed and amplified using the
513 following conditions: 95°C for 3 min, 20 cycles of denaturation at 95°C for 15 s, annealing at
514 56°C for 15 s and extension at 65°C for 6 min, and a final extension of 65°C for 6 min. The
515 resulting DNA library was purified using 0.6X Agencourt AMPure XP beads (Beckman Coulter,
516 CA, USA) and eluted in 10 µL 10 mM Tris-HCl pH 8.0, 50 mM NaCl. The library concentration
517 was determined using a Qubit 4 Fluorometer with the Qubit dsDNA HS Assay Kit (Thermo
518 Fisher Scientific, USA). Equimolar quantities of individual barcoded sample libraries were
519 pooled and the volume was adjusted to 10 µL using 10 mM Tris-HCl pH 8.0, 50 mM NaCl.
520 Subsequently, 1 µL rapid sequencing adapter (RAP) was added to the pooled library and the
521 tube was incubated at room temperature for five minutes. Then, 34 µL Sequencing Buffer, 25.5

522 µL Loading Beads, and 4.5 µL nuclease-free water were added to the tube, and the contents
523 were mixed gently. The prepared pooled library was added to a verified and primed
524 FLO-MIN106 R9.4.1 flow cell (Oxford Nanopore Technologies, UK) in a MinION (Oxford
525 Nanopore Technologies, UK) following the manufacturer's instructions. DNA sequencing was
526 conducted with default parameters using a MinIT (Oxford Nanopore Technologies, UK) with
527 MinKNOW v2.1.12 (Oxford Nanopore Technologies, UK). Fast5 files were base-called with
528 Guppy v4.0.15 using the template_r9.4.1_450bps_hac.jsn high accuracy model (Oxford
529 Nanopore Technologies, UK).

530

531 ### *1.7 Metagenomic sequences processing*

532 The initial dataset underwent demultiplexing, and primer and barcode sequences were trimmed
533 using qcat v1.1.0 (Oxford Nanopore Technologies Ltd., UK). Reads with ambiguous barcode
534 assignments were excluded from further analysis. The reads were filtered with NanoFilt v2.8.0[40]
535 to discard low-quality sequences (Q-score < 9) and sequences < 100 bp. We used the Kraken
536 v2.1.2 pipeline[41] to classify the whole metagenome shotgun sequencing reads. The reads were
537 classified using the Kraken 2 archaea, bacteria, viral, plasmid, human, UniVec_Core, protozoa,
538 and fungi reference database (k2_pluspf_20220607). To estimate relative abundances, the
539 Bracken v2.7 pipeline[42] was applied to the classification results. Subsequently, Pavian v1.0[43]
540 was used to extract abundance and taxonomic tables.

541

542 ### *1.8 Precipitation Gradient Data Analysis*

543 #### 1.8.1 Precipitation data analysis

544 To determine the differences in precipitation levels across regions, we compared the mean
545 annual precipitation in each region by fitting a linear model with the following formula:

546 Mean annual precipitation ~ Region

547

548 Differences between regions were indicated using the confidence letter display derived from
549 Tukey's *post hoc* test implemented in the package multcomp v.1.4.25[44]. We inspected the
550 normality and variance homogeneity (here and elsewhere) using Q-Q plots and the Levene test,
551 respectively. We visualized the results via a point range plot using the ggplot2 v3.5.1 R
552 package[45].

553

554 1.8.2 Soil elemental content analysis

555 For the soil elemental profile, we created a matrix in which each cell contained the calculated
556 element concentration in one sample. Then, we applied a z-score transformation to each ion
557 across the samples in the matrix. Afterward, we applied a principal component analysis (PCA)
558 using the Euclidean distance between samples and the z-score matrix as input to compare the
559 elemental profiles of soils. Additionally, we estimated the variance explained by porosity,
560 precipitation, region, and the interaction between them by performing a PERMANOVA via the
561 function *adonis2* from the vegan v.2.6-4 R package[46]. The significant variables were visualized
562 via a stacked bar plot using the *ggplot2* v3.5.1 R package.

563

564 To visualize the mineral content in each region, the z-score matrix created above was
565 hierarchically clustered (method *ward.D*, function *hclust*), and we visualized the results using a
566 heatmap. The rows in the heatmap were ordered according to the dendrogram order obtained
567 from the clustered ions, and the regions were ordered according to the precipitation gradient
568 (low precipitation to high). The heatmap was coloured based on the z-score.

569

570 To explore the relationship between ion concentrations and the precipitation gradient, we
571 performed a correlation test using *cor* function from *stats* v.4.3.1 package in R[47] of the average

z-score measurement of each ion against the precipitation gradient. Afterward, we plotted the correlation coefficient for each ion in a barplot.

1.8.3 Soil porosity analysis

The soil core images taken using x-ray computed tomography were analyzed using ImageJ v. 1.54b[48]. First, XY slice projection images were filtered using a median function to remove any noise from the raw data then an automatic threshold (Li method) was applied to produce binary images. In the binary images pores and solid particles were represented by black and white pixels, respectively. Afterwards, a region of interest (ROI) was defined in the central part of each projection to remove any potential border effect, cropping to a 600x600 pixel area. From the ROI defined in each image we extracted soil features, including particle area, perimeter, circularity, roundness, solidity, compactness, percentage of pores and pore size using the *measurement* function.

To remove the variability in the topsoil due to transportation and handling, we used two strategies. Firstly, we plotted the pore average size (mm) and soil porosity (%) for each sample. Then, we excluded from the analysis all projections having a value of soil porosity > 40% and considered the topsoil of those samples as the first projections after the exclusion. The second strategy was applied to samples with an irregular shape (e.g., mountain-like shape) at the topsoil level. We discarded all the projections with an irregular shape until we found projections with a regular distribution of soil layers. We created a data frame with the projection number (or slice) and the soil depth (projection number multiplied by the resolution). The soil porosity for each soil type was visualized via a point plot using ggplot2 v3.5.1 R package[45].

To compare the soil elemental profiles against soil porosity, first, we applied a z-score transformation of each ion and soil porosity across the samples. Then, we estimated the distance between samples using Euclidean distance. Afterwards, we contrasted the dissimilarity matrices of each pair of datasets (soil elemental profile vs. soil porosity) using the *mantel* test implemented in the vegan v.2.6-4 R package[46]. Finally, we computed the significance of the correlation between matrices by permuting the matrices 10,000 times[44].

1.8.4 Taxonomic data analysis

To compare the alpha diversity across regions, we calculated the Shannon diversity index using the diversity function from the vegan v.2.6-4 package in R[46]. We used an ANOVA to test the alpha diversity differences between regions. Differences between regions were indicated using the confidence letter display derived from Tukey's *post hoc* test implemented in the R package multcomp v.1.4.25[44].

The beta diversity analysis (Principal Coordinates Analysis, PCo) was based on Bray-Curtis dissimilarity matrices calculated using the rarefied relative abundance tables. Additionally, we estimated the variance explained by soil porosity, precipitation, regions, and the interaction between them by performing a PERMANOVA via the function adonis2 from the vegan v.2.6-4 R package[46]. The significant variables were visualized via a stacked bar plot using ggplot2 v3.5.1 R package[45].

The relative abundance of bacterial phyla was depicted using a stacked bar plot using ggplot2 v3.5.1 package.

To compare the microbiome composition against the elemental profiles and soil porosity, we contrasted the dissimilarity matrices of each pair of datasets (soil microbiome vs. soil elemental

profile and soil microbiome vs. soil porosity) using the *mantel* test implemented in the vegan v.2.6-4 R package[46]. Briefly, we calculate the microbiome dissimilarity matrix using Bray-Curtis distance. Next, we applied a z-score transformation of each ion and soil porosity across the samples. Afterward, we calculated the soil elemental dissimilarity matrix and soil porosity dissimilarity matrix using Euclidean distance. Finally, we used the *mantel* test to compare and test the significance of the correlation between matrices by permuting the matrices 10,000 times[44].

1.8.5 Heatmap and enrichment analysis

We used the R package DESeq2 v.1.40.2[49] to compute the bacterial enrichment profiles in the soils across the precipitation gradient. For each taxID (NCBI's taxonomic identifier assigned to the taxa) in the rarefied table, as well as at the species, and family levels, we estimated difference in abundance compared to the wettest collection site (Welda Prairie) using a generalized linear model (GLM) with the following design:

$$\text{Abundance} \sim \text{Region}$$

We extracted the following comparisons from the fitted model: CWR vs WEL, HAY vs WEL, KNZ vs WEL, SVR vs WEL, TRI vs WEL. A taxID, species, or family was considered statistically significant if it had a p-value < 0.05. We visualized the results using a heatmap. The rows in the heatmap were ordered according to the dendrogram obtained from the tax ID, species and family analysis. The relative abundance matrix was standardized across the significant tax ID, species, and family by using the z-score and the heatmap was coloured based on this value.

1.8.6 Identification of marker taxa associated with precipitation gradients

To identify the corresponding bacterial isolates considered as "biomarker" taxa associated with precipitation gradients, we identified the principal components (PCs) that explain more than 80% of the variance in the data. These identified PCs were used to control the effects of soil

elemental profile on the taxa abundances. Then, we fit five models: Poisson, negative binomial, two zero-inflated, and a multiple regression model.

For Poisson and negative binomial models, we fitted the following design:

Abundance ~ precipitation + offset (porosity) + offset (soil elemental profile: six first PCs)

In parallel, we fitted the zero-inflated models using the following design:

Poisson: Abundance ~ precipitation + offset (porosity) | 1 + offset (soil elemental profile) | 1

Negative binomial: Abundance ~ precipitation + porosity | porosity + soil elemental profile | soil elemental profile

Next, to assess the statistical significance, we applied ANOVA to the best-performing model for each taxon according to the Akaike Information Criterion (AIC). Additionally, we applied a multiple regression model with the following design:

Abundance ~ precipitation + porosity + soil elemental profile

Then, we applied ANOVA to find taxIDs with a significant partial regression coefficient for precipitation.

A taxa ID was considered a “marker” if it had a relative abundance > 0.01 and a prevalence > 20%. We visualized the average standardized relative abundance (z-score) of the significant taxa ID in a point plot using ggplot2 v3.5.1 package[45].

1.8.7 Enrichment of bacteria biological functions associated with precipitation gradients

To identify biological processes enriched within the microbial communities, the sequence reads were assembled into contigs for each sample using metaFlye from the Flye v2.9 package[50] with default mode. The contigs generated were then grouped and deduplicated using the dedupe.sh

674 tool in BBTools v38.76[51] to eliminate redundancies. Next, we determined the relative abundance
675 of the contigs by mapping the reads from the samples to the contigs using minimap2 v2.17[52],
676 and extracting the relative abundance counts using CoverM v0.6.1[53] in the 'contig' mode and
677 reads_per_base coverage method. Taxonomic classification of the contigs was performed using
678 the CAT v8.22 taxonomic classification pipeline[54]. Subsequently, the contigs were filtered to
679 retain only bacteria sequences. DESeq2 v1.40.0[49] was used to determine the contig enrichment
680 profiles by fitting a GLM with the following design:

681 Abundance ~ Legacy + Biological Replicate

682

683 The low-precipitation soil versus the high-precipitation soil contrast was extracted from the fitted
684 model. Contigs meeting the criteria of an FDR-adjusted *p*-value (*q*-value) <0.05 and a
685 $\log_2$-transformed fold change >2 were selected for further analysis. Open reading frames
686 encoded within the contigs were predicted using FragGeneScanRs v1.1.0[55] with default
687 settings. This was followed by functional annotation of the predicted proteins using the
688 eggNOG-mapper v2.1.9[56] pipeline with the eggNOG v5.0.2 database[57] with Diamond v2.0.11[58]
689 and MMseqs2[59].The genes annotated with Gene Ontology (GO) classifications were
690 subsequently extracted, and a GO enrichment analysis focusing on biological processes was
691 conducted. This involved employing adaptive GO clustering in conjunction with Mann–Whitney
692 U testing, using the GO_MWU tool[60], which evaluates the enrichment of each GO category
693 based on whether genes linked to the GO category are significantly clustered at either the top or
694 bottom of a globally ranked gene list. First, genes were ranked based on the signed
695 $\log_2$-transformed fold change values. For each gene, any missing parental terms for specific GO
696 categories were then automatically added. Next, fully redundant categories (those containing
697 identical sets of genes), were collapsed into the more specific GO term. To further streamline
698 the analysis, highly similar categories were grouped using complete linkage clustering based on
699 the fraction of shared genes. We used default settings, where GO categories were merged if the

700 most dissimilar pair within a group shared more than 75% of the genes in the smaller category.
701 The merged group was named after the largest category. Significantly enriched and depleted
702 GO categories were then determined by an adjusted *p*-value of <0.05. This approach simplified
703 the GO hierarchy and addressed multiple testing which improved the statistical power of the GO
704 enrichment analysis. The most prominent enriched and depleted GO categories shared across
705 comparisons were visualized in ggplot2 v3.4.2 and coloured based on the square root
706 transformed delta rank values (enrichment score) of the GO categories.

707 1.8.8 Analysis of genetic variation among bacterial lineages along the precipitation gradient

708 To assess genetic differences between bacteria lineages along the precipitation gradient, we
709 focused on 15 of the identified bacterial markers (Pseudomonas ID287, Salmonella ID28901,
710 Sorangium ID56, Bradyrhizobium ID722472, Luteitalea ID1855912, Bradyrhizobium ID1355477,
711 Flavisolibacter ID661481, Bradyrhizobium ID858422, Rubrobacter ID2653851, Bradyrhizobium
712 ID1437360, Candidatus Koribacter ID658062, Streptomyces ID1916, Klebsiella ID573,
713 Bradyrhizobium ID1325107, Edaphobacter ID2703788), as well as 18 additional abundant and
714 prevalent species (Rubrobacter ID49319, Bacillus ID1428, Bradyrhizobium ID1274631, Priestia
715 ID1404, Lacibacter ID2760713, Bradyrhizobium ID1325100, Candidatus Solibacter ID332163,
716 Burkholderia ID28450, Flavisolibacter ID1492898, Bacillus ID1396, Escherichia ID562,
717 Rhizobium ID384, Rubrobacter ID2653852, Microvirga ID2807101, Archangium ID83451,
718 Pseudomonas ID303, Paenibacillus ID1464, Nitrosospira ID1231) across the samples, as
719 proxies for the broader bacterial communities. These taxa were selected for their high genome
720 coverage across samples, enabling more precise allele frequency estimates. Reference
721 genomes for each species were retrieved from the NCBI Genome database, and the filtered
722 shotgun metagenomic reads were aligned to these genomes using minimap2 v2.17-r941[52].
723 Alignments were sorted and indexed with SAMtools v1.18[61], followed by variant calling using
724 BCFtools v1.18[62]. This process identified 23,197,278 sequence variants, which were then

filtered using VCFtools v0.1.16[63], to retain only biallelic single nucleotide polymorphisms (SNPs) for further analysis. SNP filtering criteria included a variant quality score >20, a minor allele frequency (MAF) >0.01, <50% missing data, and a minimum sequencing depth of 10x in each sample. After filtering, 23,061 high-quality biallelic SNPs were retained. Genetic distances were computed using PLINK v1.90p[64], and reduced to two dimensions through classical multidimensional scaling with the stats v4.3.0 package. PCoA plots were created with ggplot2 v3.4.2[45], colored by soil type, precipitation levels and geographical region.

To identify genes potentially under selection across the precipitation gradient, we conducted a genetic-environment association (GEA) analysis. For this, SNPs were re-filtered using VCFtools v0.1.16[63] with the same criteria, but allowing <50% missing data and a minimum sequencing depth of 5x per sample. After filtering, 93,013 biallelic SNPs were retained. Subsequently, GEA analysis was performed using a general linear model in the rMVP v1.1.1 package[65], with native SNP data imputation, and average precipitation at each sampling location as the environmental variable. The genetic structure in the data was corrected using the first 10 principal components (PCs). Manhattan plots were generated using CMplot v4.5.1[66] and significant associations were identified using the permutation method within the rMVP package.

2. Conditioning phase: Soil drought legacy is resilient to short-term perturbations

2.1 Experimental design

The six soils collected from across the Kansas precipitation gradient, as described in materials and methods 1.1, were used in this experiment. The conditioning perturbations imposed in these experiments took place over approximately 20 weeks at the University of Kansas from December 17th, 2020 to May 5th, 2021. Each of the six input soils remained independent

749 throughout the experiment. Mesocosms consisted of a 1:1 (v/v) mixture of field-collected soil to
750 sterile turface MVP (Turface Athletics, Buffalo Grove, IL). A total of 192 sterile 100 mL pots were
751 filled with the six soils and which were then randomly assigned to one of four conditions in a
752 fully-factorial design: with or without a host, and either water-stressed or well-watered. Half the
753 pots were planted with seedlings of the native prairie grass *Tripsacum dactyloides* (Eastern
754 gamagrass, cultivar "Pete"); the rest remained unplanted. These 24 treatment groups (6 soils X
755 2 water-stressed/well-watered X 2 planted/unplanted) each had *N*=8 replicates for a total of 192
756 experimental soils in pots. All mesocosms were allowed to adapt to their watering regimes in a
757 growth chamber set to a 12-hour day cycle, 27°C/23°C, and ambient humidity. Well-watered
758 control pots were watered every 1-2 days and water-stressed plants were watered every 3-5
759 days when plants displayed drought symptoms (e.g., leaf curling). All pots were fertilized with 35
760 mL of 1mL/L concentration of Bonide 10-10-10 plant food (Bonide Products LLC, Oriskany, NY)
761 on week 8 and week 12.
762

763 ### *2.2 Sample collection*

764 To characterize the baseline microbial communities going into the conditioning treatments, we
765 sampled four replicates of each soil/treatment combination one week after beginning the
766 experiment. To collect the samples, the top centimeter of soil was discarded and the remaining
767 soil was homogenized to ensure even sampling of the top, middle, and bottom of the pot. Two
768 grams of this homogenized soil were placed in a 15mL tube, flash-frozen in liquid nitrogen, and
769 stored at -80°C for microbial DNA and RNA extraction. To characterize the effects of the four
770 treatments on the microbial communities, we sampled all remaining replicates at the end of the
771 20-week conditioning phase. Soil samples were collected as described for the baseline
772 communities, but an additional 6 g of homogenized soil was preserved at 4°C in 50 mL conical
773 tubes for use as inocula in a downstream experiment. Additionally, for the planted pots, we

774 measured *T. dactyloides* shoot height before uprooting the plants. We collected samples of a
775 crown root from each plant (3 cm long each, beginning 2 cm from the base of the plant) and
776 stored them in 50% ethanol at 4°C for downstream laser ablation tomography analysis. The
777 remaining roots and shoots were dried in an oven at 225°C for 12 hours and then weighed
778 separately.
779
780 *2.3 Changes in bacterial community structure associated with drought and well-watered*
781 *conditioning with and without a host.*

782 2.3.1 DNA extraction

783 Total DNA was extracted from baseline and post-conditioning soil sub-samples using the DNA
784 Set for NucleoBond RNA Soil Kit (Macherey-Nagel, Düren, Germany) according to the
785 manufacturer's instructions.
786

787 2.3.2 Library preparation and sequencing

788 DNA sequencing libraries were prepared using the Rapid PCR Barcoding Kit (SQK-RPB004)
789 from Oxford Nanopore Technologies, UK, and sequenced on a FLO-MIN106 R9.4.1 flow cell
790 (Oxford Nanopore Technologies, UK) in a MinION (Oxford Nanopore Technologies, UK), with a
791 MinIT (Oxford Nanopore Technologies, UK) using MinKNOW v2.1.12[67] (Oxford Nanopore
792 Technologies, UK) as described in materials and methods section 1.6.

793 2.3.3 Sequence processing

794 Raw sequence data were demultiplexed and primer and barcode sequences were trimmed
795 using qcat v1.1.0 (Oxford Nanopore Technologies Ltd., UK). Reads with ambiguous barcode
796 assignments were excluded from further analysis. The reads were filtered with NanoFilt v2.8.0[40]
797 to discard low-quality sequences (Q-score <9) and sequences <100 bp. We used the Kraken

798 v2.1.2 pipeline[41] for classifying the whole metagenome shotgun sequencing reads. The reads
799 were classified using the Kraken 2 archaea, bacteria, viral, plasmid, human, UniVec_Core,
800 protozoa and fungi reference database (k2_pluspf_20220607). To estimate relative
801 abundances, the Bracken v2.7 pipeline[42] was applied to the classification results. Subsequently,
802 Pavian v1.0[43] facilitated the extraction of abundance and taxonomic tables. Functions in
803 phyloseq v1.44.0[68] with microbiome v1.22.0 and microbiomeutilities v1.0.17[69] were used to filter
804 the dataset and remove samples with low read depth (<1000 reads), remove unidentified taxa
805 and singletons, transform abundance values using rarefaction, subset and merge sample and
806 taxonomic groups and perform other data frame manipulations.

807 *2.4 Plant biomass*

808 Root and shoots were detached, dried in an oven at 225˚C for 12 hours, and then weighed.

809

810 *2.5 Root Laser Ablation Tomography (LAT) analysis*

811 We collected samples of a crown root from each plant (3 cm long each, beginning 2 cm from the
812 base of the plant) and stored them in 50% ethanol at 4°C. The samples were shipped to the
813 University of Nottingham for downstream LAT analysis. Briefly, root segments were dehydrated
814 in 100% methanol for 48 hours, transferred to 100% ethanol for 48 hours, then dried with an
815 automated critical point dryer (CPD, Leica EM CPD 300, Leica Microsystem). Root anatomical
816 images were acquired using a laser ablation tomograph (LATScan, Lasers for Innovative
817 Solutions LLC). This utilises a combination of precise positioning stages with a guided pulsed
818 UV (355 nm) laser, to thermally vaporise thin sections of the root, and then to illuminate the
819 exposed surface. The tomograph was retrofitted with a microscopic imaging system, using a
820 machine vision camera unit (Model Grasshopper3, FLIR) and infinity-corrected long working
821 distance magnifying objectives (Mitutoyo (UK) Ltd.)

822

823 *2.6 Changes in gamagrass morphological features under drought and well-water conditioning*

824 To identify morphological features in gamagrass that changed with the conditioning (drought and
825 well-watered) treatments, we used Image J to quantify the average area aerenchyma, number
826 aerenchyma, number metaxylem, cortical cell layers, total area metaxylem, average area
827 metaxylem, stele min. diameter, stele max. diameter, stele area, stele perimeter, total area
828 aerenchyma, adjusted cortex area, root min. diameter, cortex min. diameter, root max. diameter,
829 cortex max. diameter, total perimeter, cortex perimeter, root total area, and cortex area.
830 Additionally, we quantified the root-shoot ratio, number of leaves, number of green leaves, root
831 mass, shoot mass, and shoot height.

832

833 *2.7 Metatranscriptome analysis*

834 2.7.1 RNA isolation

835 Total RNA was extracted from baseline and post-conditioning soil sub-samples with the
836 NucleoBond RNA Soil Kit (Macherey-Nagel, Düren, Germany) using the manufacturer's
837 instructions. Isolated RNA was treated with Turbo DNA-free (Applied Biosystems, Waltham, MA,
838 USA) to remove contaminating DNA, following the manufacturer's instructions.

839

840 2.7.2 Library preparation and sequencing

841 RNA libraries were prepared using 1 µg of total RNA according to established protocols with
842 modifications. Briefly, poly(A)-tail-containing RNA was removed from the RNA samples using
843 Sera-mag oligo(dT) magnetic beads (GE Healthcare Life Sciences, Marlborough, MA, USA) and
844 then the samples were subjected to ribodepletion with the NEBNext rRNA Depletion Kit (New
845 England Biolabs, MA, USA), following the manufacturers' instructions. The purified RNA was
846 resuspended in a fragmentation mix consisting of 6.25 µL Milli-Q water, 5 µL 5x First strand
847 buffer, and 1.25 µL random primers (3 µg/µL) and fragmented at 94°C for 6 min. First-strand

848 cDNA synthesis was performed using a mixture of 0.8 µL reverse transcriptase, 2 µL 100 mM
849 DTT, 0.4 µL 25 mM dNTP, 0.5 µL RNAseOUT (40U/µL), 10 µL RNA, and 6.3 µL Milli-Q water.
850 The reactions were incubated at 25°C for 10 min, 42°C for 50 min, and 70°C for 15 min.
851 Second-strand cDNA synthesis was performed by adding a master mix of 18.4 µL Milli-Q water,
852 5 µL 10X second strand buffer, 1.2 µL 25 mM dNTP, 0.4 µL RNAse H (5U/µL), and 5 µL DNA
853 Pol I (10U/µL) to the sample, followed by incubation at 16°C for 1 h. The samples were then
854 purified using Agencourt AMPure XP beads. Subsequently, the libraries were end-repaired with
855 a mixture of 30 µL sample, 2.5 µL of 3 U/µL T4 DNA polymerase, 0.5 µL of 5 U/µL Klenow DNA
856 polymerase, 2.5 µL of 10 U/µL T4 PNK, 5 µL of 10X T4 DNA ligase buffer with 10 mM ATP, 0.8
857 µL of 25 mM dNTP mix, and 8.7 µL Milli-Q water, incubated at 20°C for 30 min, and purified
858 again using Agencourt AMPure XP beads. Following this, the RNA libraries were adenylated in
859 a mix containing 34 µL of the end-repaired sample, 3 µL of 5 U/µL Klenow exo-, 5 µL of 10X
860 Enzymatics Blue Buffer, 1 µL of 10 mM dATP, and 9 µL of Milli-Q water. The mixture was
861 incubated at 37°C for 30 min, followed by 70°C for 5 min, and then purified using Agencourt
862 AMPure XP beads. Individual samples were indexed through ligation using a mix of 10.25 µL
863 sample, 1 µL of 600 U/µL T4 DNA ligase, 12.5 µL of 2x Rapid Ligation Buffer, and 1.25 µL of 2.5
864 µM indexing adapter from the KAPA Dual-Indexed Adapter Kit (Kapa Biosystems, MA, USA).
865 The samples were incubated at 25°C for 15 min, followed by the addition of 5 µL of 0.5 M EDTA
866 pH 8. The libraries were purified twice with Agencourt AMPure XP beads. The libraries were
867 enriched in a reaction containing 20 µL sample, 25 µL of 2X KAPA HiFi HS Mix (Kapa
868 Biosystems, MA, USA), 2.5 µL of 5 µM I5 primer, and 2.5 µL of 5 µM I7 primer. The reactions
869 were initially heated to 98°C for 45 seconds, followed by 14 cycles of 98°C for 15 seconds, 60°C
870 for 30 seconds, and 72°C for 30 seconds, with a final extension at 72°C for 1 minute. The
871 resulting RNA libraries were purified using Agencourt AMPure XP beads, quantified on a Qubit
872 4 Fluorometer (Thermo Fisher Scientific, USA), and the library size was assessed using High
873 Sensitivity D1000 ScreenTape on the Agilent 4200 TapeStation (Agilent Technologies, Santa

874 Clara, CA). Equimolar quantities of individual barcoded RNA libraries were pooled in a
875 randomized manner and shipped on dry ice to Beijing Genomics Institute (BGI, Shenzhen,
876 China). Each library pool was sequenced on an MGI Tech MGISEQ-2000 sequencing platform
877 to generate a minimum of 10 million 100 bp paired-end reads per sample.
878
879 *2.7.3 Taxonomic classification of transcripts*
880 Cutadapt v4.6[70] was used to remove primer and barcode sequences and low-quality sequences
881 from the paired-end reads of the sequenced RNA libraries. To identify taxa with enriched gene
882 expression activity, the reads were classified using the Kraken v2.1.2 pipeline[41] with the
883 archaea, bacteria, viral, plasmid, human, UniVec_Core, protozoa and fungi reference database
884 (k2_pluspf_20220607), and the Bracken v2.7 pipeline[42] was applied to the classification results
885 to estimate the relative abundances. The counts table was generated from Pavian v1.0[43]. Data
886 filtering and statistical analysis were then performed as before using phyloseq v1.44.0[68] with
887 microbiome v1.22.0[71] and microbiomeutilities v1.0.17[69].
888

889 ***2.8 Data Analysis***

890 2.8.1 Changes in bacterial community structure associated with drought and well-watered
891 conditioning with and without a host
892 To assess the alpha diversity across the samples, we calculated the Shannon Diversity Index
893 using phyloseq v1.44.0[68]. We used ANOVA to test for significant differences in Shannon
894 Diversity indices between groups and means were separated using Tukey's honestly significant
895 difference (HSD) test from the agricolae v1.3.5 R package[72]. For beta diversity, Bray-Curtis
896 dissimilarity matrices were calculated using phyloseq v1.44.0 and the variance explained by
897 legacy, conditioning, and host were estimated by performing permutational multivariate analysis
898 of variance (PERMANOVA) using the adonis2 function in vegan v2.6.4 R package[46].

Constrained ordination of beta-diversity was plotted using canonical analysis of principal coordinates (CAP) based on Bray-Curtis dissimilarity matrices calculated with vegan v2.6.4. We visualized differences with the CAP analysis, using the following models:

~ legacy + Condition (conditioning + host + biological replicate)

~ conditioning + Condition (legacy + host + biological replicate)

~ host + Condition (legacy + conditioning + biological replicate)

The relative abundance of taxa was plotted as a stacked bar representation using phyloseq v1.44.0. The tax_glom function in phyloseq v1.44.0 was used to agglomerate taxa, and the aggregate_rare function in microbiome v1.22.0 was used to aggregate rare groups. We used DESeq2 v1.40.0[49] to calculate the enrichment profiles by fitting a generalized linear model (GLM) with the following design:

Abundance ~ Legacy + Conditioning + Biological Replicate

We extracted the following comparisons from the fitted model: wet soil legacy with watered conditioning vs wet soil legacy (baseline), wet soil legacy with drought conditioning vs wet soil legacy (baseline), dry soil legacy (baseline) vs wet soil legacy (baseline), dry soil legacy with watered conditioning vs wet soil legacy (baseline), and dry soil legacy with drought conditioning vs wet soil legacy (baseline). Taxa were considered significant if they had an FDR-adjusted *p*-value (*q*-value) <0.05. The results of the GLM analysis were rendered in heatmaps, coloured based on the $\log_2$-transformed fold change output by the GLM. Significant differences between comparisons with a *q*-value <0.05 with $\log_2$-transformed fold change >2 were highlighted with black squares.

Relative abundances of the taxonomic markers were extracted, and an ANOVA was performed to assess significant differences between treatment groups. Tukey's Honest Significant

925 Difference (HSD) test, implemented using the agricolae v1.3.5 R package[72], was used for
926 post-hoc pairwise comparisons. To further explore the effects of watering and drought
927 treatments, with and without a host, on the relative abundances of the taxonomic markers, we
928 subset the data and applied a generalized linear model (GLM) using DESeq2 v1.40.0[49]. The
929 model was structured as follows:

930 Abundance ~ Legacy + Conditioning + Host + Biological Replicate

931

932 We then extracted the following comparisons from the fitted model for each soil legacy: water
933 conditioning vs baseline, drought conditioning vs baseline, water conditioning with host vs
934 baseline, drought conditioning with host vs baseline. Markers were considered significant if the
935 FDR-adjusted p-value (q-value) was < 0.05. Results from the GLM analysis were visualized in a
936 heatmap, with colours representing log2-transformed fold changes. Comparisons showing
937 significant differences (q-value <0.05 and log2-transformed fold change >2) were highlighted
938 with black squares.

939

940 *2.8.2 Gene Ontology (GO) term enrichment analysis*

941 To identify enriched biological processes within the microbial communities, sequence reads from
942 individual samples were assembled into contigs using metaFlye from the Flye v2.9 package[50]
943 with default parameters, as described in Methods Section 1.8.7. Relative abundance counts
944 were then determined, and the resulting contigs were subjected to taxonomic classification and
945 filtering, also as outlined in Methods Section 1.8.7. We used DESeq2 v1.40.0[49] to determine the
946 bacterial contig enrichment profiles by fitting a generalized linear model (GLM) with the following
947 design:

948 Abundance ~ Legacy + Conditioning + Biological Replica

949

950 We extracted the following comparisons from the fitted model: wet soil legacy with watered
951 conditioning vs wet soil legacy (baseline), wet soil legacy with drought conditioning vs wet soil
952 legacy (baseline), dry soil legacy (baseline) vs wet soil legacy (baseline), dry soil legacy with
953 watered conditioning vs wet soil legacy (baseline), and dry soil legacy with drought conditioning
954 vs wet soil legacy (baseline). Contigs meeting the criteria of an FDR-adjusted *p*-value (*q*-value)
955 < 0.05 and a $\log_2$-transformed fold change > 2 were selected. Open reading frames were
956 predicted and functionally annotated, and genes with GO classifications were subjected to GO
957 enrichment analysis with the GO_MWU tool[60].
958

959 2.8.3 Changes in gamagrass morphological features under drought and well-water condition

960 For each root feature identified, we used ANOVA to test for significant differences between
961 groups and means were separated using Tukey's honestly significant difference (HSD) test from
962 the agricolae v1.3.5 R package[72] Subsequently, the feature values were normalized using the
963 rescale function from the scales v1.2.1 R package. The mean normalized feature values were
964 then visually represented on a heatmap using ggplot2 v3.4.2. Subsequently, Pearson correlation
965 coefficients between these features and corresponding *p*-values were computed using the rcorr
966 function from the Hmisc v5.0.1 package[73]. The results of the correlation analysis were
967 graphically presented using ggplot2 v3.4.2, where the colour of the plots reflected the
968 correlation coefficient values. Significant correlations (p <0.05) were emphasized with black
969 squares on the plots. Furthermore, the coefficient of variation for the feature values was
970 calculated and depicted using ggplot2 v3.4.2. The three plots were integrated based on the
971 hierarchical clustering of the Pearson correlation coefficients of the features. The clustering
972 employed the ward.D2 method within the hclust function in R, utilizing Euclidean distances
973 calculated using the dist function.
974

975 2.8.4 Metatranscriptome sequence analysis

976 To assess transcriptional differences in the activity of the bacterial community, Bray-Curtis
977 dissimilarity matrices were calculated. The variance explained by legacy, conditioning, and host
978 was estimated using permutational multivariate analysis of variance (PERMANOVA) with the
979 adonis2 function from the vegan v2.6.4 R package[46]. Beta-diversity patterns were visualized
980 through constrained ordination using canonical analysis of principal coordinates (CAP). We
981 applied CAP analysis to visualize differences using the following models:

982 ~ Legacy + Condition (conditioning + host + biological replicate)

983 ~ Conditioning + Condition (legacy + host + biological replicate)

984 ~ Host + Condition (legacy + conditioning + biological replicate)

985

986 Transcriptional activity among taxa was displayed as a stacked bar plot using phyloseq v1.44.0.
987 We employed DESeq2 v1.40.0[49] to calculate enrichment profiles by fitting a generalized linear
988 model (GLM) with the following design:

989 Abundance ~ Legacy + Conditioning + Biological Replicate

990

991 From the fitted model, we extracted the following comparisons: wet soil legacy with watered
992 conditioning vs wet soil legacy (baseline), wet soil legacy with drought conditioning vs wet soil
993 legacy (baseline), dry soil legacy (baseline) vs wet soil legacy (baseline), dry soil legacy with
994 watered conditioning vs wet soil legacy (baseline), and dry soil legacy with drought conditioning
995 vs wet soil legacy (baseline). Taxa were considered differentially abundant if the FDR-adjusted
996 *p*-value (*q*-value) was <0.05. Results from the GLM analysis were visualized in heatmaps,
997 where colours represent log2-transformed fold changes. Comparisons showing significant
998 differences (*q*-value <0.05 and log2-transformed fold change >2) were highlighted with black
999 squares.

1000

1001 Additionally, high-quality filtered reads of the transcriptome were de novo assembled into a
1002 reference metatranscriptome using Trinity v2.15.1[74] with default parameters. Open reading
1003 frames in transcripts were predicted with TransDecoder v5.7.1[75] with default settings. Functional
1004 annotation of the predicted proteins was performed using the eggNOG-mapper v2.1.9[56] pipeline,
1005 utilising the eggNOG v5.0.2 database[57] with Diamond v2.0.11[58] and MMseqs2[59]. The taxonomic
1006 classification of transcripts was conducted using the CAT v8.22 taxonomic classification
1007 pipeline[54]. Sequence reads were further filtered using SortMeRNA v4.3.6[76] with the
1008 smr_v4.3_default_db.fasta database to remove residual amplified rRNA sequences. Transcript
1009 quantification analysis was performed using Salmon v1.10.0 in the mapping-based mode with
1010 the de novo assembled reference metatranscriptome. Subsequently, the transcript-level
1011 abundance estimates from salmon were extracted for the identified transcripts using the R
1012 package tximport v1.28.044 as raw counts in default setting[77]. DESeq2 v1.40.0[49] was utilized to
1013 determine the bacterial transcript enrichment profiles by fitting a generalised linear model (GLM)
1014 as described before. Genes meeting the criteria of an FDR-adjusted *p*-value (*q*-value) <0.05, a
1015 $\log_2$-transformed fold change >2, and had GO classifications, were subjected to GO enrichment
1016 analysis with the GO_MWU tool[60].

1017

1018 2.8.5 Analysis of genetic variation among bacterial lineages

1019 Filtered shotgun metagenomic reads were aligned to the reference genomes of 33 selected
1020 taxa, including 22 identified bacterial markers and 11 additional abundant and prevalent species
1021 (see Supplementary Materials and Methods 1.8.8), using Minimap2 v2.17-r941[52]. The resulting
1022 alignments were sorted and indexed with SAMtools v1.18[61]. Variant calling was performed using
1023 BCFtools v1.18[62], and variants were filtered with VCFtools v0.1.16[63]. Filtering criteria included a
1024 variant quality score >20, a minor allele frequency (MAF) >0.01, <50% missing data, and a

1025 minimum sequencing depth of 10x in each sample. After filtering, a total of 8,293 high-quality
1026 biallelic SNPs were available for further analysis. To assess genetic variation within and
1027 between groups, we analysed molecular variance (AMOVA) using poppr v2.9.6[78]. The
1028 significance of the AMOVA results was determined with a permutation test using the randtest
1029 function in ade4 v1.7.22[79]. To determine the extent of genetic differentiation between groups, we
1030 calculated the Fixation index (FST) values using the hierfstat v0.5.11[80] package. Principal
1031 coordinates analysis (PCoA) plots were generated as previously described in Supplementary
1032 Materials and Methods 1.8.8, and coloured to reflect soil legacy, drought/ well-watered and host/
1033 no-host treatments. To identify genes associated with soil legacy, we conducted a genome-wide
1034 association study (GWAS). SNPs were re-filtered using VCFtools v0.1.16[63], applying the same
1035 criteria but allowing for up to 70% missing data and a minimum sequencing depth of 3x in each
1036 sample. GWAS was conducted using a general linear model in the rMVP v1.1.1 package[65].
1037 Associations were identified by comparing bacterial lineages from dry legacy soil to those from
1038 wet legacy soil. Genetic structure was accounted for by incorporating the first 10 principal
1039 components. Significant associations were identified through permutation testing within the
1040 rMVP package, and Manhattan plots were generated using CMplot v4.5.1[66].
1041

1042 **3. Test phase: Effects of soil microbiome legacy on plant tolerance to drought**

1043 *3.1 Experimental design and non-destructive phenotypic measurements*

1044 At the end of the "Conditioning Phase", homogenized soil was collected from each pot by
1045 discarding the top one centimeter of soil, mixing the soil in the pot with a clean plastic spatula,
1046 and placing six grams in a sterile 50 mL conical tube. For rhizosphere samples (i.e., planted
1047 pots), plants were gently pulled from the pots and the soil particles adhered to and within the
1048 root bundle were shaken into a sterile 50 mL conical tube. The rhizosphere particles were
1049 homogenized with a clean plastic spatula and particles were poured out of the tube until six
1050 grams remained. Soil and rhizosphere samples were stored at 4˚C overnight.

1051

1052 Soil microbes were extracted from the 6 g soil or rhizosphere sample the following day by
1053 adding 25 mL of autoclaved 1X PBS with 0.0001% Tween-89 to the 50 mL tube containing the
1054 sample. Tubes were vigorously shaken to mix and break up large soil aggregates. Large
1055 particles were allowed to settle to the bottom of the tube; the supernatant was then filtered
1056 through autoclaved Miracloth (Sigma-Aldrich) into a new sterile 50 mL conical tube. Filtered
1057 samples were then centrifuged at 3600g for 25 min at 4˚C. The supernatant was discarded, and
1058 the microbial pellet was resuspended in 6 mL of 1X PBS buffer using a vortex. The resuspended
1059 pellets were stored at 4˚C until used for inoculations a few hours later.

1060

1061 As stated in section 2.1, the conditioning phase had 24 treatment groups with eight replicates of
1062 each treatment (192 pots total). For the test phase, microbial extracts from all eight replicates of
1063 each group (plus sterile buffer-only control inoculums) were each inoculated into a pot planted
1064 with gamagrass (N=200) and a pot planted with maize (N=200) that were then maintained under
1065 watered-stress (drought) conditions. Furthermore, four of the eight replicate extracted microbial
1066 inoculants (as well as four sterile buffer-only control inoculums) were each inoculated into an
1067 additional gamagrass planted (N=100) and maize planted (N=100) pots, which were then
1068 maintained under well watered control conditions. This makes for a total of N=600 plants at the
1069 start of the test phase. Throughout the experiment, nine water-stressed maize and five
1070 well-watered maize were lost (no gamagrass died). Therefore, phenotype measurements were
1071 completed on a total of N=586 plants. We chose this design because resource and space
1072 limitations prevented us from testing all 192 inocula under both drought and control conditions,
1073 and we were primarily interested in microbial effects on plant function under drought; we
1074 therefore opted to maximize our power to test for differences among the inocula under water
1075 limitations.

1076

1077 To create the inoculum, the resuspended pellet was inverted three times to mix and 1 mL of the
1078 sample was added to 100 mL of sterile 0.5X MS liquid medium, for a microbial titer equivalent to
1079 0.01 g soil per mL. The “mock inoculation” controls were created by substituting 1 mL of sterile
1080 PBS for the resuspended microbial pellet. Finally, 25 mL of this suspension was inoculated onto
1081 the soil surface of each Test Phase pot. Thus, each microbial community extracted from one of
1082 the 192 conditioning phase pots was used to inoculate either two or four plants in the Test
1083 Phase. To maintain statistical independence of the experimental replicates from the conditioning
1084 phase, no pooling was performed.
1085
1086 Before inoculation, pots were planted with 3-4-day old gamagrass or maize germinants.
1087 Gamagrass seeds were soaked in 3% hydrogen peroxide for 24 hours and germinated in seed
1088 trays filled with sterile clay. Maize seeds were soaked in 70% ethanol for 3 minutes, then soaked
1089 in 5% NaClO on a rotator for 2 min, and then rinsed with sterile DI water three times. Treated
1090 maize seeds were germinated on sterile damp paper towels inside sealed plastic bags.
1091
1092 Pots were fully randomized and, prior to inoculation, were filled with a homogenized 5:1 (w/w)
1093 mixture of all-purpose sand (TechMix All-purpose 110241) and calcined clay (Pro's choice rapid
1094 dry) that had been sterilized by autoclaving on a one-hour liquid cycle. Pots were autoclaved on
1095 a 30 min liquid cycle and then filled with the sand:clay mixture, leaving one inch of room at the
1096 top of the pot. To help keep the mixture from falling out of the drain holes in the bottom of the
1097 pots, a sterile filter paper was shaped into a cone, pushed to the bottom of the pot, and a sterile
1098 marble was used to weigh the paper down. This effectively blocked the substrate, but still
1099 allowed water to exit the drainage holes. Plants were grown under 12-h days, 27°C/23°C
1100 (day/night), and ambient humidity, with the light setting set to 1, which is equivalent to 312
1101 $\mu mol/m^2s$. Three-day old gamagrass and maize leaf photosynthetic rates and gas exchange
1102 were measured using the LI-6800 (LI-COR, Lincoln, NE, USA), across 3 days for each host.

1103 The LI-6800 aperture was 2 cm, warmup tests were performed at the start of each
1104 measurement session, the Fluorometry was set to “on”, the APD_Leaf to set to 1.5 kpa. The
1105 newest fully emerged leaf, which was most commonly the 4th leaf, on each plant was clamped
1106 in the chamber and allowed to stabilize until all measurements were stable for at least 30 secs
1107 before the measurements were recorded, which took approximately five minutes per leaf.
1108 Similarly, the leaf chlorophyll content was also measured using the MC-100 Chlorophyll
1109 Concentration Meter (apogee instruments, Logan, UT, USA).

1110 Maize plants were sampled four weeks after planting and gamagrass was sampled five
1111 weeks after planting. In total, we measured 300 T. dactyloides plants (200 droughted, 100
1112 well-watered) and 286 maize plants (191 droughted, 95 well-watered).

1113

1114 At the end of the Test Phase, uprooted plants were gently shaken to remove the soil attached to
1115 roots, prior to the collection of phenotypic, transcriptomic, and microbiome data as described
1116 below. One crown root was cut off with a ceramic blade and placed in a 1.7 mL tube on dry ice
1117 for downstream DNA extraction for 16S rRNA gene sequencing. Another crown root (0.15 - 0.2
1118 g) was cut off with a ceramic blade, placed in a 1.7 mL tube, and flash frozen in liquid nitrogen
1119 for downstream RNA extraction. In between plants, the ceramic blade, plastic tweezers, plastic
1120 cutting board, and gloves were cleaned with 30% bleach. All samples were held on dry ice and
1121 then transferred to a -80˚C freezer for storage. Next, the root and shoot were separated with a
1122 ceramic blade. Three cm of crown root beginning ~2 cm from the base of the shoot was cut with
1123 a ceramic blade and submerged in 50% EtOH for LAT analysis. The rest of the root system was
1124 submerged in 70% EtOH in a 50 mL centrifuge tube for downstream root architecture scanning.
1125 Shoot height and number of leaves were recorded. Shoots were placed in individual paper
1126 bags, dried in an oven at 225˚C for 12 hours, and the shoot dry weight was recorded.

1127

1128 *3.2 Root system architecture and root biomass analyses*

1129 A Perfection V600 flatbed scanner (Epson, Nagano, Japan) was used to scan intact maize and
1130 gamagrass root systems collected from Test Phase plants. The scanner was set to professional
1131 mode, reflective, document, black and white mode, 600 dpi, with a threshold of 55. A clear
1132 plastic tray filled with clean water was placed on the scanning bed. Each root system was
1133 placed in the tray with water and the tangled roots were gently pulled apart using plastic
1134 tweezers until they were no longer overlapping. A small amount of fine fibrous roots that fell off
1135 during this process were pushed to the corner of the tray and not included in the root cluster
1136 scan. The scanned root images were then analyzed using Rhizovision Explorer software v.
1137 2.0.3[81] in "whole root" mode and converted to 600 dpi. The region of interest tool was used to
1138 outline the main root bundle before pressing play to collect feature measurements. Finally, after
1139 collection of root system architecture data, the roots were dried in an oven at 225˚C for 12 hours
1140 and then weighed.

1141

1142 *3.3 Root Laser Ablation Tomography (LAT) analysis*

1143 We collected one crown root from each plant (3 cm long each, beginning 2 cm from the base of
1144 the plant) and stored them in 50% ethanol at 4°C. These samples were shipped to the
1145 University of Nottingham for LAT analysis. Briefly, root segments were dried with an automated
1146 critical point dryer (CPD, Leica EM CPD 300, Leica Microsystem). Then, samples were ablated
1147 by a laser beam (Avia 7000, 355 nm pulsed laser) to vaporize the root tissue at the camera focal
1148 plane ahead of an imaging stage and cross-sectional images were taken using a Canon T3i
1149 camera with a 5×micro-lens (MP-E 65 mm) on the laser-illuminated surface. ImageJ software[48]
1150 was used to measure root anatomical traits captured in the high-quality LAT images.

1151

1152 *3.4 Leaf ionome and shoot biomass analyses*

1153 The elemental profiles of the shoots were measured using Inductively Coupled Plasma Mass
1154 Spectrometry (ICP-MS). The shoot biomass from all uprooted plants was dried in an oven at

1155 225°C for 12 h and then weighed. The dried biomass samples were cut into small pieces using
1156 a clean ceramic scalpel and placed in 5 mL Eppendorf tubes with 3 zirconium oxide beads.
1157 Shoots were pulverized using a Tissue Lyzer II (Qiagen) using 2 cycles of 60 seconds at the
1158 frequency of 30 s^{-1}. Next, 5-10 mg of pulverized shoot samples were weighted on a Mettler
1159 five-decimal analytical scale, and 1-3 mL (depending on the sample dry weight) of concentrated
1160 trace metal grade nitric acid Primar Plus (Fisher Chemicals) was added to each tube. Prior to
1161 the digestion, 20 µg/L of Indium (In) was added to the nitric acid as an internal standard to
1162 assess putative errors in dilution or variations in sample introduction and plasma stability in the
1163 ICP-MS instrument. The samples were then digested in DigiPREP MS dry block heaters (SCP
1164 Science; QMX Laboratories) for 4 h at 115°C. After cooling down, the digested samples were
1165 diluted to 10-30 mL (depending on the volume of the nitric acid added) with 18.2 MΩcm Milli-Q
1166 Direct water. The elemental analysis was performed using an ICP-MS, PerkinElmer NexION
1167 2000 equipped with Elemental Scientific Inc 4DXX FAST Dual Rinse autosampler, FAST valve
1168 and peristaltic pump. The instrument was fitted with a PFA-ST3 MicroFlow nebulizer, baffled
1169 cyclonic C3 high sensitivity glass spray chamber cooled to 2 ºC with PC3X Peltier heated/cooled
1170 inlet system, 2.0 mm i.d. quartz injector torch and a set of nickel cones. Twenty-four elements
1171 were monitored including the following stable isotopes: ^{7}Li, ^{11}B, ^{23}Na, ^{24}Mg, ^{31}P, ^{34}S, ^{39}K, ^{43}Ca,
1172 ^{48}Ti, ^{52}Cr, ^{55}Mn, ^{56}Fe, ^{59}Co, ^{60}Ni, ^{63}Cu, ^{66}Zn, ^{75}As, ^{82}Se, ^{85}Rb, ^{88}Sr, ^{98}Mo, ^{111}Cd, ^{208}Pb and ^{115}In.
1173 Helium was used as a collision gas in Kinetic Energy Discrimination mode (KED) at a flow rate
1174 of 4.5 mL/min while measuring Na, Mg, P, S, K, Ca, Ti, Cr, Mn, Fe, Ni, Cu, Zn, As, Se and Pb to
1175 exclude possible polyatomic interferences.
1176
1177 The remaining elements were measured in the standard mode. The instrument Syngistix™
1178 software for ICP-MS v.2.3 (Perkin Elmer) automatically corrected any isobaric interferences. The
1179 ICP-MS measurements were performed in peak hopping scan mode with dwell times ranging
1180 from 25 to 50 ms depending on the element, 20 sweeps per reading and three replicates. The

1181 ICP-MS conditions were adjusted to an RF power of 1600 Watts and an auxiliary gas flow rate
1182 of 1.20 L/min. Torch alignment, nebuliser gas flow and quadrupole ion deflector (QID) voltages
1183 (in standard and KED mode) were optimized before analysis for highest intensities and lowest
1184 interferences (oxides and doubly charged ions levels lower than 2.5%) with NexION Setup
1185 Solution containing 1 µg/L of Be, Ce, Fe, In, Li, Mg, Pb and U in 1% nitric acid using a standard
1186 built-in software procedure. To correct for variation between and within ICP-MS analysis runs,
1187 liquid reference material was prepared using pooled digested samples and run after the
1188 instrument calibration and then after every nine samples in all ICP-MS sample sets. Equipment
1189 calibration was performed at the beginning of each analytical run using seven multi-element
1190 calibration standards (containing 2 µg/L In internal standard) prepared by diluting 1000 mg/L
1191 single-element standards solutions (Inorganic Ventures; Essex Scientific Laboratory Supplies
1192 Ltd) with 10% nitric acid. As a calibration blank, 10% nitric acid containing 2 µg/L In internal
1193 standard was used, and it was run throughout the analysis. Sample concentrations were
1194 calculated using the external calibration method within the instrument software. Further data
1195 processing, including the calculation of final element concentrations, was performed in Microsoft
1196 Excel.
1197

1198 ### *3.5 Crown root transcriptomics*

1199 #### 3.5.1 RNA extraction and sequencing

1200 For RNA extractions and sequencing, flash-frozen crown roots were freeze-dried for 48 hours
1201 and finely ground with pellet pestles. The RNA extraction protocol was carried out according to
1202 the NucleoSpin RNA Plant kit (Macherey-Nagel, Düren, Germany).
1203

1204 For the 132 maize samples, remnant DNA was removed from purified RNA using the DNA-Free
1205 kit (Invitrogen, Carlsbad, CA, USA). RNA-seq libraries were prepared using the QuantSeq 3'

1206 mRNA-Seq V2 kit with unique dual sequences and the unique molecular identifier (UMI) module
1207 (Lexogen, Vienna, Austria) following the manufacturer's recommendations. Libraries were
1208 pooled at equimolar concentrations and then sequenced (2x150bp, but reverse reads were not
1209 used) on a NovaSeq S4 flow cell (Illumina, San Diego, CA, USA) along with a 25% PhiX
1210 spike-in. Maize RNA-seq library preparations and sequencing were performed by the RTSF
1211 Genomics Core at Michigan State University. For the 132 *T. dactyloides* samples, RNA-seq
1212 libraries were prepared using the NEBNext Ultra II Directional Library Kit with the oligo-dT
1213 magnetic isolation module (New England Biolabs, Ipswich, MA, USA) and sequenced on the
1214 Illumina NovaSeq 6000 platform at the Genomic Sciences Laboratory at North Carolina State
1215 University to generate a minimum of 40M read pairs (2x150bp) per sample.

1216 ### 3.5.2 Sequence processing

1217 For the maize sequence reads, UMIs were removed from all sequences and added to the read
1218 headers using UMI-tools[82]. Next, cutadapt version 4.2[70] was used to remove the first four bases
1219 of each read, remove poly-A tails (if present), remove spurious poly-G runs using the
1220 --nextseq-trim=10 parameter, and remove adapter sequences. Reads that were <10 bp long or
1221 that aligned to maize rRNA gene sequences were removed; the remaining reads were aligned
1222 to the maize reference genome B73 RefGen_v5[83] using HISAT2 version 2.2.1[84]. Aligned reads
1223 were converted to BAM format, sorted, and indexed using samtools version 1.9[61]. We then used
1224 UMI-tools[82] to de-duplicate reads that both shared a UMI and had identical mapping
1225 coordinates. Finally, we used the FeatureCounts function of the subread package version 2.0.5[85]
1226 with the maize genome annotation version Zm00001eb.1 and parameters -O --fraction -M
1227 --primary -g ID -t gene to generate a table of transcript counts.
1228
1229 For the *T. dactyloides* sequence reads, we first used cutadapt to remove NEBNext adapter
1230 sequences, poly-A tails, spurious poly-G runs, and low-quality tails using the -q 20,20 parameter

1231 and other default parameters. The cleaned reads were aligned to the *T. dactyloides* reference
1232 genome (Td-KS_B6_1-REFERENCE-PanAnd-2.0a[61] using HISAT2. The alignments were
1233 name-sorted so that mate-pairs could be fixed using the fixmate function of samtools[61], and then
1234 re-sorted based on coordinates, de-duplicated, and converted to indexed BAM files using the
1235 same software. Finally, a table of transcript expression estimates was generated using the
1236 FeatureCounts function of the subread package with parameters -p -O --fraction -M --primary -g
1237 ID -t gene and the *T. dactyloides* genome annotation version
1238 Td-KS_B6_1-REFERENCE-PanAnd-2.0a_Td00002ba.2.

1239 3.5.3 Statistical analyses

1240 Because the maize and *T. dactyloides* RNA-seq datasets were generated using different
1241 approaches (3' tag sequencing *vs.* full-length sequencing, respectively) we analyzed them in
1242 parallel rather than comparing them directly. For each species, we used DESeq2[49] to identify
1243 genes that were differentially expressed between plants inoculated with microbiomes from a
1244 low-precipitation climate ("dry legacy") *vs.* those inoculated with microbiomes from a
1245 high-precipitation climate ("wet legacy"). A single negative binomial model with default
1246 parameters was used to estimate $\log_2$-fold changes in gene expression due to inoculum legacy,
1247 while also controlling for the other experimental factors, using the model:

1248 Counts ~ Legacy + ConditioningPhaseWater + ConditioningPhaseHost + TestPhaseWater

1249

1250 Statistical support was obtained using the Wald test with Benjamini-Hochberg FDR correction.
1251 All available samples were included in each analysis; thus, these results should be interpreted
1252 as the gene expression response to microbiome precipitation legacy, averaged across all levels
1253 of the other experimental factors.

1254

1255 In addition, we investigated whether plants' gene expression responses to limited *vs.* ample
1256 water during the Test Phase were affected by inoculum precipitation legacy. To do so, we used
1257 DESeq2 to fit a model with the formula:

1258 Counts ~TestPhaseWater*Legacy

1259

1260 Then, we extracted the estimated $\log_2$-fold changes due to acute drought (relative to
1261 well-watered conditions) for both dry-legacy-inoculated and wet-legacy-inoculated plants. We
1262 inferred a meaningful interaction between these variables when the 95% confidence intervals of
1263 the two drought-induced $\log_2$-fold changes did not overlap at all. These interacting genes are
1264 candidates for linking real-time plant drought response to the microbiome's historical
1265 environmental conditions.

1266

1267 Finally, we conducted a mediation analysis to determine whether the *T. dactyloides* genes that
1268 were sensitive to inoculum legacy were implicated in phenotypic responses to subsequent acute
1269 drought. A gene was considered legacy-sensitive if its expression was significantly affected by
1270 the main effect of inoculum legacy, or if it was affected by the interaction between inoculum
1271 legacy and test phase drought treatment, as described above. We summarized expression
1272 patterns of this subset of genes (normalized as transcripts per million, calculated using the full
1273 set of expressed genes) using non-metric multidimensional scaling of the Bray-Curtis distances
1274 among all *T. dactyloides* plants, which resulted in two axes of variation: MDS1 and MDS2. Next,
1275 we used the mediation package in R[86] to compare the direct effects of test phase drought
1276 treatment on each focal plant trait (see section *3.7.1. Plant trait feature selection*) to the indirect
1277 effects of the drought treatment mediated through MDS1 and MDS2. Each mediation analysis
1278 used the linear models:

1279 Trait value ~ MDS + Test phase drought treatment

1280 MDS ~ Test phase drought treatment

where MDS represents the “site score” of each individual plant on either MDS1 or MDS2. Separate models were fit to test the potential roles of MDS1 and MDS2 as mediator variables; however, a follow-up analysis using both MDS1 and MDS2 as simultaneous mediators, implemented in lavaan[87], yielded equivalent conclusions.

3.5.4 Gene annotation

We downloaded maize and eastern gamagrass genome assemblies and annotations from MaizeGDB[83,88]. Functional information for maize genes was taken from the *Zea mays* genome annotation version Zm-B73-REFERENCE-NAM-5.0_Zm00001eb.1 and accessed using MaizeGDB’s MaizeMine tool[83,88–90]. For *Tripsacum dactyloides* genes, we relied on DNA sequence homology with annotated maize genes to infer function. We used BEDtools[91] to extract gene coordinates and protein-coding sequences from the *T. dactyloides* reference genome Td-KS_B6_1-REFERENCE-PanAnd-2.0a[92], and then used OrthoFinder[93] to compare coding sequences from the two species. OrthoFinder identified 32,785 *T. dactyloides* genes (71.5% of the total) as homologs of maize genes, grouping them into 21,658 distinct orthogroups. All differential gene expression analyses, however, considered the entire set of expressed genes; those without maize orthologs, or with unannotated maize orthologs, were considered to be of unknown function.

3.6 16S rRNA amplicon sequencing

3.6.1 DNA extractions and library preparation

One crown root from each plant was cut off with a ceramic blade and placed in a 1.7 mL tube and flash frozen in liquid nitrogen for downstream amplicon library preparation. After collection, root sub-samples were kept on dry ice and ceramic tweezers were used to transfer the whole root to 1.1 mL cluster tubes (USA Scientific, Ocala, FL, USA). Tweezers were sterilized with

1306 80% EtOH between samples. Roots were selected at random for placement in cluster tubes and
1307 were stored at -80ºC until DNA extraction, at which time roots were freeze-dried for 48 hours in
1308 a FreeZone lyophilizer (Labconco, Kansas City, MO, USA). After freeze-drying, roots were flash
1309 frozen in liquid nitrogen. To break apart thick roots, sterile forceps and a dissecting needle were
1310 used before placing the rack of cluster tubes in an HT Lysing Homogenizer (OHAUS,
1311 Parsippany, NJ, USA) with two clean 5/32" steel balls in each tube. Samples were homogenized
1312 at 25 Hz for 1 min. Root material was then transferred to 2 mL bead-beating 96-well plates
1313 containing sterile 1 mm garnet beads with 850 µL of lysis buffer (1M Tris, pH = 8.0; 100 mM
1314 NaCl; 10 mM EDTA).
1315
1316 A positive (ZymoBiomics Microbial Community Standard) and negative control, (800 µL of lysis
1317 buffer) were included on each plate. Bead-beating plates were stored at -20ºC until extraction.
1318 After thawing, 10 µL of 20% sodium dodecyl sulfate (SDS) was added to each well before
1319 homogenizing for a total of 20 min at 20 Hz. Plates were incubated in a water bath (55ºC for 90
1320 min) and centrifuged (6 min at 4500 x g). 400 µL of the resulting supernatant was transferred to
1321 new 1 mL 96-well plates containing 120 µL of 5 M potassium acetate in each well and incubated
1322 overnight at -20ºC. After thawing the plates, they were centrifuged (6 min at 4500 x g) and 400
1323 µL of the supernatant was transferred to a new 1 mL 96-well plate containing 600 µL of diluted
1324 SPRI-bead solution (protocol derived from[94]). These plates were mixed thoroughly for 5 min at
1325 1000 r.p.m. on an orbital plate shaker. Samples were allowed to incubate for 10 min so DNA
1326 could bind to beads, after which the plate was centrifuged (6 min at 4500 x g) and placed on a
1327 magnet rack for 10 min. The supernatant was removed, and the beads were washed twice with
1328 900 µL of 80% EtOH. After washing, the supernatant was decanted and the beads were
1329 air-dried. DNA was eluted in 75 µL of pre-heated 1x TE (pH = 7.5; 37ºC) and transferred to
1330 clean 0.45 mL plates and stored at -20ºC.
1331

1332 16S-v4 rRNA gene amplification was performed using paired 515f/806r primers[95,96]. PCR
1333 reactions contained DreamTaq Master Mix (Thermo Fisher Scientific, Waltham, MA, USA), 10
1334 mg/µL bovine serum albumin (BSA), 100 µM peptide nucleic acid (PNA), and PCR-grade water.
1335 BSA was used to enhance PCR amplification while PNA was used to suppress primer binding
1336 and subsequent amplification of mitochondrial and chloroplast 16S regions[97]. The PCR included
1337 an initial denaturation step at 95ºC for 2 min, followed by 27 cycles of an additional denaturation
1338 at 95ºC for 20 s, PNA annealing at 78ºC for 5 s, primer annealing at 52ºC for 20 s, and
1339 extension at 72ºC for 50 s. This was followed by a final extension step for 10 min at 72ºC. PCR
1340 products were purified by incubating at 37ºC for 20 min and then 15 min at 80ºC after mixing
1341 with 0.78 µL of PCR-grade water, 0.02 µL of 10 U/µL exonuclease I (Applied Biosystems), and
1342 0.2 µL of 1U/µL shrimp alkaline phosphatase (Applied Biosystems) per 10 µL PCR product. Two
1343 µL of the purified amplicons were used as template DNA in an indexing PCR to attach barcoded
1344 P5 and P7 Illumina adaptors. The 10 µL reaction included 5 µM each of P5 and P7 adaptors, 1x
1345 DreamTaq Master Mix (Thermo Fisher Scientific), 10 mg/mL BSA, 100 µM PNA, and PCR-grade
1346 water. An initial denaturation step was performed at 95ºC for 2 min. For 8 cycles, an additional
1347 denaturation was carried out at 95ºC for 20 s, PNA annealing at 78ºC for 5 s, primer annealing
1348 at 52ºC for 20 s, and extension at 72ºC for 50 s. A final extension step was performed at 72ºC
1349 for 10 min. PCR products were verified via 2% agarose gel electrophoresis and then pooled by
1350 96-well plate using the “Just-a-Plate” PCR cleanup and normalization kit (Charm Biotech, St.
1351 Louis, MO, USA). Pools were size selected and combined in equimolar concentrations before
1352 being sequenced on an Illumina SP flow cell on the NovaSeq 6000 platform (2x250bp reads).
1353

1354 ### 3.6.2 Amplicon data processing

1355 We removed primer sequences from raw 16S-v4 Illumina reads using cutadapt[70], requiring at
1356 least 5 nucleotides of overlap. Additional quality control and processing was performed with the

DADA2 software[98]. Forward reads were discarded if they had more than 6 expected errors, otherwise they were truncated at 200 nucleotides; for reverse reads the parameters were 7 expected errors and 170 nucleotides. Error rates were estimated separately for forward and reverse reads based on a sample of $1x10^8$ bases, then used to denoise and dereplicate reads using the standard DADA2 functions. Chimeric sequences were detected and removed using the “consensus” procedure in DADA2. Each individual sample was processed in parallel, after which all of the resulting amplicon sequence variant (ASV) tables were merged. Finally, taxonomy of each ASV was assigned by comparison to the RDP database[99].

3.6.3 Root bacterial community diversity analysis

All statistical analyses were performed using R (v4.4.0). Unfortunately, some samples were lost due to a 96-well plate being dropped during the sample DNA extraction and due to filtering of samples based on sequence quality. Ultimately, 156 gamagrass root microbiome and 276 maize root microbiome samples were included in these analyses. The cleaned and prepared microbiome data, as phyloseq objects, were loaded into R[68]. The phyloseq object sample data table was replaced with an updated metadata file. The “mock” samples were removed from the dataset and the data was subset by the test phase host, maize and gamagrass using phyloseq::subset_samples (v1.48.0). Maize and gamagrass root bacterial microbiome Shannon Diversity was fit to a mixed-effects model using the lme4 (v1.1-35.4) package[100] and lmer() function, using the following model:

$$expShannon \sim TestWater + Legacy + (1|DNAplate)$$

A type III ANOVA was performed using stats::anova()[101] to test for significance, followed by pairwise comparisons and significance tests using emmeans (v1.10.2) package[102] with false discovery rate adjustments. Data visualizations were generated using ggplot2 (v3.5.1)[45], the

error bars represent standard error and the points are estimated marginal means. All plots were saved in PDF format. Composite figures were created in Adobe Illustrator.

Bacterial community beta diversity was accessed with a Constrained Analysis of Principal Coordinates, using phyloseq::ordinate, method="CAP", and distance="Euclidean" with the following formula:

~TestWater+Legacy+Condition(DNAplate)+Condition(CondHost)+
Condition(CondWater)

An ANOVA-like permutation test was used to test for model significance using the vegan::anova.cca() function[46]. The anova.cca by=term option was used to determine the significance of the TestWater and Legacy variables separately. CAP1 and CAP2 axes were plotted using ggplot2, including 95% confidence interval ellipse (stat_ellipse()). To evaluate treatment group beta-dispersion, Euclidean distances were calculated for the centered-log ratio transformed counts using phyloseq::distance(). Both "Legacy" and "TestWater" terms were tested for beta-dispersion differences using the Euclidean distances matrix and vegan::betadisper() and vegan::permutest() to test for significance[46]. Distances were then extracted from the results output and fit to a linear model. Estimated marginal means were calculated and plotted using the same methods as above. The error bars represent standard errors.

Then, an ASV differential abundance analysis was performed on gamagrass- and maize-associated ASVs separately. Centered-log ratio transformed counts of ASVs were each fit to a linear model using an iterative for-loop. Each ASV was subset using phyloseq:subset_taxa and the phyloseq::psmelt() function was used to reformat the phyloseq object into a data frame. Then the ASV abundance was fit to the following model:

$$\text{Abundance} \sim \text{Legacy*TestWater}$$

Then, stats::anova() was used to test for significance, followed by an FDR p-value adjustment using stats::p.adjust(). ASVs with significant (≤0.05) adjusted p-values for the Legacy*TestWater interaction terms were extracted and z-scores of the center-log ration transformed counts were plotted in a heatmap using pheatmap::pheatmap()[103] with clustering_method="complete".

3.7 Plant trait data analyses

3.7.1 Plant trait feature selection

All plant data was loaded into RStudio. The intrinsic water use efficiency (iWUE) was calculated using the ratio of photosynthetic rate (A) and stomatal conductance (gs) or A/gs ((μmol m^{-2} s^{-1})/(mol m^{-2} s^{-1})). Data was subset by Test Phase host treatment groups (gamagrass and maize). For the feature selection, the "mock" treatment was removed. The 67 features that were selected for testing were subset into a data frame. Three sample rows were removed from the dataset because they had missing data. The drought susceptibility index (S-index) was calculated for each of these features using the following formula:

$$S=\text{Trait}_{\text{drought}}/\text{mean}(\text{Trait}_{\text{control}})$$

Then, for each host, a random forest model was used to select the top 10 most important features from the 67 total s-index measurements using randomForest()[104], with "Legacy" as the predictor. Correlations (stats::cor()) were estimated for the top ten traits and if any two of the top 10 traits were highly correlated ($r \geq 0.7$), the trait that ranked lower in the random forest model was removed. Non-correlative top features from the test water treatment groups (drought vs. watered control) were combined for each test phase host (maize and gamagrass). Vegan:rda() was used to perform a redundancy analysis on the top features using the following formula:

Top_features~ Legacy + Condition(CondGroup), scale=TRUE

3.7.2 Feature analyses

An ANOVA-like permutation test was used to test for model significance using the vegan::anova.cca() function. A biplot was created using ggplot2 plotting RDA1 and PC1 axes, as well as the species scores (represented by arrows), and stat_ellipse was used to plot 95% confidence intervals of the site scores.

Finally, s-indices for each of the top features and iWUE were fit to mixed-effects models, when possible, or a fixed-effects model if overfitting of the mixed effects model occurred. Each feature or trait was visually assessed for outliers, which were removed. Removing the outliers did not impact the interpretation of any of the results. Formulas used for the mixed effects or linear model, respectively, include:

lmer(s-index ~ Legacy + (1|CondGroup))

lm(s-index ~ Legacy + CondGroup)

The fit of the model was accessed and if needed, the s-index was transformed using sqrt(), exp(), or log() to improve the fit. ANOVA was used to assess significance and estimated marginal means were calculated and plotted as described above.

Data availability

The *16S rRNA* gene amplicon sequencing data, shotgun metagenomic data, and metatranscriptome data associated with this study have been deposited in the NCBI Sequence Read Archive under the BioProject IDs PRJNA1267293, PRJNA1267715, PRJNA1268489, and

PRJNA1186942. The raw RNA-seq data from gamagrass and maize have been deposited in the Gene Expression Omnibus under accessions GSE282586 and GSE282587, respectively.

Code availability

We deposited all scripts and additional data structures required to reproduce the results of this study in a Zenodo repository (http://doi.org/10.5281/zenodo.13821006). Source data are provided in the Zenodo repository and with this paper.

Acknowledgements

We thank Dr. Arun Seetharam, Dr. Toby Kellogg, Dr. Matthew Hufford, and the PanAnd consortium for granting early access to the *Tripsacum dactyloides* genome and annotation. We thank Dr. Mitch Greer, Michaela VonLintel, Justin Roemer, Dr. Alan Schlegel, and the Nature Conservancy for granting access to soil collection sites in Kansas, and Dr. Peter Balint-Kurti for providing maize seeds. We thank Dr Craig J. Sturrock and Dr Brian S. Atkinson from the Hounsfield Facility at the University of Nottingham for their assistance with the analysis of the CT images. We are grateful to the undergraduate student researchers and technicians who helped to set up experiments and collect data: Felicity Tso, Hannah Reid, and Carmen Rodriguez. Thank you to Dr. Joel Swift, Ceyda Kural-Rendon, Dr. Ben Sikes (University of Kansas), Dr. Manuel Kleiner (North Carolina State University), Dr Omri Finkel (The Hebrew University of Jerusalem, Israel), and Dr Nicholas Girkin (University of Nottingham, UK) for critical reading of the manuscript. This work was supported by a UKRI/BBSRC - NSF/BIO Lead Agency Opportunity, National Science Foundation award #IOS-2016351 and BBSRC grant #BB/V011294/1. Maize root transcriptome library preps and sequencing were performed in the RTSF Genomics Core at Michigan State University. *T. dactyloides* library preps and RNA-seq were performed at the NC State University Genomic Sciences Laboratory (Raleigh, NC, USA).

Research reported in this publication was made possible in part by the services of the KU Genome Sequencing Core. This lab is supported by the National Institute of General Medical Sciences (NIGMS) of the National Institutes of Health under award number P30GM145499. We thank the University of Kansas Medical Center – Genomics Core for generating the 16S amplicon sequence data sets. The Genomics Core is supported by the Kansas Intellectual and Developmental Disabilities Research Center (NIH U54 HD 090216), the Molecular Regulation of Cell Development and Differentiation – COBRE (P30 GM122731), The NIH S10 High End Instrumentation Grant (NIH S10OD021743) and the Frontiers CTSA Grant (UL1TR002366).

Author contributions

Conceptualization: N.A.G., V.C., D.G., G.C., and M.R.W. Data curation: N.A.G., V.C., D.G., and M.R.W.; Formal analysis: N.A.G., V.C., D.G., I.S.-G., and M.R.W.; Investigation: N.A.G., V.C., D.G., N.F., D.D.J., D.M.W., A.M., G.C., and M.R.W.; Methodology: G.C. and M.R.W.; Project administration: G.C. and M.R.W.; Software: N.A.G., V.C., D.G., and M.R.W.; Supervision: G.C. and M.R.W.; Visualization: N.A.G., V.C., D.G., and M.R.W.; Writing – original draft: N.A.G., G.C., and M.R.W.; Writing – review & editing: V.C. and D.G.

Competing interests

The authors declare no competing interests.

References

1. Chase, A. B., Weihe, C. & Martiny, J. B. H. Adaptive differentiation and rapid evolution of a

soil bacterium along a climate gradient. *Proc. Natl. Acad. Sci. U. S. A.* **118**, (2021).

2. Lau, J. A. & Lennon, J. T. Rapid responses of soil microorganisms improve plant fitness in novel environments. *Proc. Natl. Acad. Sci. U. S. A.* **109**, 14058–14062 (2012).

3. Canarini, A. *et al.* Ecological memory of recurrent drought modifies soil processes via changes in soil microbial community. *Nat. Commun.* **12**, 5308 (2021).

4. Naylor, D., DeGraaf, S., Purdom, E. & Coleman-Derr, D. Drought and host selection influence bacterial community dynamics in the grass root microbiome. *ISME J.* **11**, 2691–2704 (2017).

5. Custódio, V. *et al.* Sculpting the soil microbiota. *Plant J.* **109**, 508–522 (2022).

6. Liu, Z. *et al.* Shifts in microbial communities and networks are correlated with the soil ionome in a kiwifruit orchard under different fertilization regimes. *Appl. Soil Ecol.* **149**, 103517 (2020).

7. Dai, Z. *et al.* Metallic micronutrients are associated with the structure and function of the soil microbiome. *Nat. Commun.* **14**, 8456 (2023).

8. Stewart, B. W., Capo, R. C. & Chadwick, O. A. Effects of rainfall on weathering rate, base cation provenance, and Sr isotope composition of Hawaiian soils. *Geochim. Cosmochim. Acta* **65**, 1087–1099 (2001).

9. Sverdrup, H. Chemical weathering of soil minerals and the role of biological processes. *Fungal Biol. Rev.* **23**, 94–100 (2009).

10. Guellouz, L., Askri, B., Jaffré, J. & Bouhlila, R. Estimation of the soil hydraulic properties from field data by solving an inverse problem. *Sci. Rep.* **10**, 9359 (2020).

11. Rousseva, S., Torri, D. & Pagliai, M. Effect of rain on the macroporosity at the soil surface. *Eur. J. Soil Sci.* **53**, 83–93 (2002).

12. Schimel, J. P. Life in dry soils: Effects of drought on soil microbial communities and processes. *Annu. Rev. Ecol. Evol. Syst.* **49**, 409–432 (2018).

13. Sun, Y., Wilkinson, B. J., Standiford, T. J., Akinbi, H. T. & O'Riordan, M. X. D. Fatty acids

1526 regulate stress resistance and virulence factor production for Listeria monocytogenes. *J.*
1527 *Bacteriol.* **194**, 5274–5284 (2012).
1528 14. Woodcock, S. D. *et al.* Trehalose and α-glucan mediate distinct abiotic stress responses in
1529 Pseudomonas aeruginosa. *PLoS Genet.* **17**, e1009524 (2021).
1530 15. Gil-Quintana, E. *et al.* Local inhibition of nitrogen fixation and nodule metabolism in
1531 drought-stressed soybean. *J. Exp. Bot.* **64**, 2171–2182 (2013).
1532 16. Singh, S. *et al.* Aldehyde dehydrogenases in cellular responses to oxidative/electrophilic
1533 stress. *Free Radic. Biol. Med.* **56**, 89–101 (2013).
1534 17. Lebre, P. H., De Maayer, P. & Cowan, D. A. Xerotolerant bacteria: surviving through a dry
1535 spell. *Nat. Rev. Microbiol.* **15**, 285–296 (2017).
1536 18. Gury, J. *et al.* Inactivation of PadR, the repressor of the phenolic acid stress response, by
1537 molecular interaction with Usp1, a universal stress protein from Lactobacillus plantarum, in
1538 Escherichia coli. *Appl. Environ. Microbiol.* **75**, 5273–5283 (2009).
1539 19. Sharma, P., Jha, A. B., Dubey, R. S. & Pessarakli, M. Reactive oxygen species, oxidative
1540 damage, and antioxidative defense mechanism in plants under stressful conditions. *J. Bot.*
1541 **2012**, 1–26 (2012).
1542 20. Yuda, E. *et al.* Mapping the key residues of SufB and SufD essential for biosynthesis of
1543 iron-sulfur clusters. *Sci. Rep.* **7**, 9387 (2017).
1544 21. Parsons, J. B. & Rock, C. O. Bacterial lipids: metabolism and membrane homeostasis.
1545 *Prog. Lipid Res.* **52**, 249–276 (2013).
1546 22. Zhu, J., Brown, K. M. & Lynch, J. P. Root cortical aerenchyma improves the drought
1547 tolerance of maize (*Zea mays* L.). *Plant Cell Environ.* **33**, 740–749 (2010).
1548 23. Gao, Y. & Lynch, J. P. Reduced crown root number improves water acquisition under water
1549 deficit stress in maize (Zea mays L.). *J. Exp. Bot.* **67**, 4545–4557 (2016).
1550 24. Ahmed, M. A. *et al.* Root type matters: measurement of water uptake by seminal, crown,
1551 and lateral roots in maize. *J. Exp. Bot.* **69**, 1199–1206 (2018).

1552 25. Swift, J. F. *et al.* Drought stress homogenizes maize growth responses to diverse natural
1553 soil microbiomes. *Plant Soil* (2024) doi:10.1007/s11104-024-06853-x.
1554 26. Springer, T. L. & Dewald, C. L. Eastern gamagrass and other *Tripsacum* species. in
1555 *Warm-Season (C4) Grasses* 955–973 (American Society of Agronomy, Crop Science
1556 Society of America, Soil Science Society of America, Madison, WI, USA, 2016).
1557 27. Batstone, R. T., O'Brien, A. M., Harrison, T. L. & Frederickson, M. E. Experimental evolution
1558 makes microbes more cooperative with their local host genotype. *Science* **370**, 476–478
1559 (2020).
1560 28. Morella, N. M. *et al.* Successive passaging of a plant-associated microbiome reveals robust
1561 habitat and host genotype-dependent selection. *Proceedings of the National Academy of*
1562 *Sciences* **117**, 1148–1159 (2020).
1563 29. Hund, A., Ruta, N. & Liedgens, M. Rooting depth and water use efficiency of tropical maize
1564 inbred lines, differing in drought tolerance. *Plant Soil* **318**, 311–325 (2009).
1565 30. Schulz, P. *et al.* Improving plant drought tolerance and growth under water limitation
1566 through combinatorial engineering of signalling networks. *Plant Biotechnol. J.* **19**, 74–86
1567 (2021).
1568 31. Lebeis, S. L. *et al.* PLANT MICROBIOME. Salicylic acid modulates colonization of the root
1569 microbiome by specific bacterial taxa. *Science* **349**, 860–864 (2015).
1570 32. Zhou, M.-L. *et al.* Nicotianamine synthase gene family as central components in heavy
1571 metal and phytohormone response in maize. *Funct. Integr. Genomics* **13**, 229–239 (2013).
1572 33. Lee, D.-K. *et al.* The rice OsNAC6 transcription factor orchestrates multiple molecular
1573 mechanisms involving root structural adaptions and nicotianamine biosynthesis for drought
1574 tolerance. *Plant Biotechnol. J.* **15**, 754–764 (2017).
1575 34. Zhang, Z.-X. & Zheng, Y.-Z. Overexpression of nicotianamine synthase (NAS) gene results
1576 in enhanced drought tolerance in perennial Ryegrass. *Biotechnol. Biotechnol. Equip.* **22**,
1577 938–941 (2008).

35. Chaumont, F., Barrieu, F., Wojcik, E., Chrispeels, M. J. & Jung, R. Aquaporins constitute a large and highly divergent protein family in maize. *Plant Physiol.* **125**, 1206–1215 (2001).

36. de Vries, F., Lau, J., Hawkes, C. & Semchenko, M. Plant–soil feedback under drought: does history shape the future? *Trends Ecol. Evol.* **38**, 708–718 (2023).

37. Evans, S., Allison, S. & Hawkes, C. Microbes, memory and moisture: Predicting microbial moisture responses and their impact on carbon cycling. *Funct. Ecol.* (2022) doi:10.1111/1365-2435.14034.

38. Stackhouse, P. Nasa power. https://power.larc.nasa.gov/.

39. Soltanpour, P. N. & Schwab, A. P. A new soil test for simultaneous extraction of macro- and micro-nutrients in alkaline soils. *Commun. Soil Sci. Plant Anal.* **8**, 195–207 (1977).

40. De Coster, W., D'Hert, S., Schultz, D. T., Cruts, M. & Van Broeckhoven, C. NanoPack: visualizing and processing long-read sequencing data. *Bioinformatics* **34**, 2666–2669 (2018).

41. Wood, D. E., Lu, J. & Langmead, B. Improved metagenomic analysis with Kraken 2. (2019) doi:10.1101/762302.

42. Lu, J., Breitwieser, F. P., Thielen, P. & Salzberg, S. L. Bracken: estimating species abundance in metagenomics data. *PeerJ Comput. Sci.* **3**, e104 (2017).

43. Breitwieser, F. P. & Salzberg, S. L. Pavian: interactive analysis of metagenomics data for microbiome studies and pathogen identification. *Bioinformatics* **36**, 1303–1304 (2020).

44. Hothorn, T., Bretz, F. & Westfall, P. Simultaneous inference in general parametric models. *Biom. J.* **50**, 346–363 (2008).

45. Wickham, H. *Ggplot2: Elegant Graphics for Data Analysis*. (Springer, Berlin, Germany, 2016).

46. Oksanen, J. *et al.* vegan : Community Ecology Package. R package version 1.8-5. (2007).

47. The R Project for Statistical Computing. http://www.R-project.org/.

48. Schneider, C. A., Rasband, W. S. & Eliceiri, K. W. NIH Image to ImageJ: 25 years of image

1604 analysis. *Nat. Methods* **9**, 671–675 (2012).

1605 49. Love, M. I., Huber, W. & Anders, S. Moderated estimation of fold change and dispersion for
1606 RNA-seq data with DESeq2. *Genome Biol.* **15**, 550 (2014).

1607 50. Kolmogorov, M. *et al.* metaFlye: scalable long-read metagenome assembly using repeat
1608 graphs. *Nat. Methods* **17**, 1103–1110 (2020).

1609 51. BBTools. *DOE Joint Genome Institute* https://jgi.doe.gov/data-and-tools/bbtools/ (2016).

1610 52. Li, H. Minimap2: pairwise alignment for nucleotide sequences. *Bioinformatics* **34**,
1611 3094–3100 (2018).

1612 53. Woodcroft, B. J. *CoverM: Read Coverage Calculator for Metagenomics*. (Github).

1613 54. von Meijenfeldt, F. A. B., Arkhipova, K., Cambuy, D. D., Coutinho, F. H. & Dutilh, B. E.
1614 Robust taxonomic classification of uncharted microbial sequences and bins with CAT and
1615 BAT. *Genome Biol.* **20**, 217 (2019).

1616 55. Van der Jeugt, F., Dawyndt, P. & Mesuere, B. FragGeneScanRs: faster gene prediction for
1617 short reads. *BMC Bioinformatics* **23**, 198 (2022).

1618 56. Cantalapiedra, C. P., Hernández-Plaza, A., Letunic, I., Bork, P. & Huerta-Cepas, J.
1619 eggNOG-mapper v2: Functional Annotation, Orthology Assignments, and Domain
1620 Prediction at the Metagenomic Scale. *Mol. Biol. Evol.* **38**, 5825–5829 (2021).

1621 57. Huerta-Cepas, J. *et al.* eggNOG 5.0: a hierarchical, functionally and phylogenetically
1622 annotated orthology resource based on 5090 organisms and 2502 viruses. *Nucleic Acids*
1623 *Res.* **47**, D309–D314 (2019).

1624 58. Buchfink, B., Reuter, K. & Drost, H.-G. Sensitive protein alignments at tree-of-life scale
1625 using DIAMOND. *Nat. Methods* **18**, 366–368 (2021).

1626 59. Steinegger, M. & Söding, J. MMseqs2 enables sensitive protein sequence searching for the
1627 analysis of massive data sets. *Nat. Biotechnol.* **35**, 1026–1028 (2017).

1628 60. Wright, R. M., Aglyamova, G. V., Meyer, E. & Matz, M. V. Gene expression associated with
1629 white syndromes in a reef building coral, Acropora hyacinthus. *BMC Genomics* **16**, 371

(2015).

61. Li, H. *et al.* The Sequence Alignment/Map format and SAMtools. *Bioinformatics* **25**, 2078–2079 (2009).

62. Danecek, P. *et al.* Twelve years of SAMtools and BCFtools. *Gigascience* **10**, (2021).

63. Danecek, P. *et al.* The variant call format and VCFtools. *Bioinformatics* **27**, 2156–2158 (2011).

64. Chang, C. C. *et al.* Second-generation PLINK: rising to the challenge of larger and richer datasets. *Gigascience* **4**, 7 (2015).

65. Yin, L. *et al.* RMVP: A memory-efficient, visualization-enhanced, and parallel-accelerated tool for genome-wide association study. *Genomics Proteomics Bioinformatics* **19**, 619–628 (2021).

66. LiLin-Yin. CMplot: Circle Manhattan Plot. *CRAN: Contributed Packages* The R Foundation https://doi.org/10.32614/cran.package.cmplot (2015).

67. Faisal, M., Silander, O. & Freed, N. Starting a MinION sequencing run using MinKNOW v1. (2020) doi:10.17504/protocols.io.bfwqjpdw.

68. McMurdie, P. J. & Holmes, S. phyloseq: an R package for reproducible interactive analysis and graphics of microbiome census data. *PLoS One* **8**, e61217 (2013).

69. Shetty, S. Lahti L. microbiomeutilities: microbiomeutilities: Utilities for Microbiome Analytics. 2022. Preprint at (2023).

70. Martin, M. Cutadapt removes adapter sequences from high-throughput sequencing reads. *EMBnet.journal* **17**, 10–12 (2011).

71. Shetty, S. A. & Lahti, L. Microbiome data science. *J. Biosci.* **44**, (2019).

72. De Mendiburu, F. & Simon, R. Agricolae - Ten years of an open source statistical tool for experiments in breeding, agriculture and biology. *PeerJ* (2015) doi:10.7287/peerj.preprints.1404.

73. The Hmisc and rms Packages. in *Biostatistics and Computer-based Analysis of Health Data*

1656 *using R* 173–186 (Elsevier, 2016).

1657 74. Grabherr, M. G. *et al.* Full-length transcriptome assembly from RNA-Seq data without a
1658 reference genome. *Nat. Biotechnol.* **29**, 644–652 (2011).

1659 75. Haas, B. J. *et al.* De novo transcript sequence reconstruction from RNA-seq using the
1660 Trinity platform for reference generation and analysis. *Nat. Protoc.* **8**, 1494–1512 (2013).

1661 76. Kopylova, E., Noé, L. & Touzet, H. SortMeRNA: fast and accurate filtering of ribosomal
1662 RNAs in metatranscriptomic data. *Bioinformatics* **28**, 3211–3217 (2012).

1663 77. Soneson, C., Love, M. I. & Robinson, M. D. Differential analyses for RNA-seq:
1664 transcript-level estimates improve gene-level inferences. *F1000Res.* **4**, 1521 (2015).

1665 78. Kamvar, Z. N., Tabima, J. F. & Grünwald, N. J. Poppr: an R package for genetic analysis of
1666 populations with clonal, partially clonal, and/or sexual reproduction. *PeerJ* **2**, e281 (2014).

1667 79. Thioulouse, J. *et al. Multivariate Analysis of Ecological Data with ade4*. (Springer, New
1668 York, NY, 2019).

1669 80. Goudet, J. hierfstat, a package for r to compute and test hierarchical *F*-statistics. *Mol. Ecol.*
1670 *Notes* **5**, 184–186 (2005).

1671 81. Seethepalli, A. *et al.* RhizoVision Explorer: open-source software for root image analysis
1672 and measurement standardization. *AoB Plants* **13**, lab056 (2021).

1673 82. Smith, T., Heger, A. & Sudbery, I. UMI-tools: modeling sequencing errors in Unique
1674 Molecular Identifiers to improve quantification accuracy. *Genome Res.* **27**, 491–499 (2017).

1675 83. Hufford, M. B. *et al.* De novo assembly, annotation, and comparative analysis of 26 diverse
1676 maize genomes. *Science* **373**, 655–662 (2021).

1677 84. Guo, J., Gao, J. & Liu, Z. HISAT2 parallelization method based on Spark cluster. *J. Phys.*
1678 *Conf. Ser.* **2179**, 012038 (2022).

1679 85. Liao, Y., Smyth, G. K. & Shi, W. featureCounts: an efficient general purpose program for
1680 assigning sequence reads to genomic features. *Bioinformatics* **30**, 923–930 (2014).

1681 86. Yimer, B. B., Lunt, M., Beasley, M., Macfarlane, G. J. & McBeth, J. BayesGmed: An

1682 R-package for Bayesian causal mediation analysis. *PLoS One* **18**, e0287037 (2023).
1683 87. Rosseel, Y. lavaan: An R Package for Structural Equation Modeling. *J. Stat. Softw.* **48**, 1–36
1684 (2012).
1685 88. Portwood, J. L., 2nd *et al.* MaizeGDB 2018: the maize multi-genome genetics and
1686 genomics database. *Nucleic Acids Res.* **47**, D1146–D1154 (2019).
1687 89. Woodhouse, M. R. *et al.* A pan-genomic approach to genome databases using maize as a
1688 model system. *BMC Plant Biol.* **21**, 385 (2021).
1689 90. Shamimuzzaman, M. *et al.* MaizeMine: A Data Mining Warehouse for the Maize Genetics
1690 and Genomics Database. *Front. Plant Sci.* **11**, 592730 (2020).
1691 91. Quinlan, A. R. BEDTools: The Swiss-Army Tool for Genome Feature Analysis. *Curr. Protoc.*
1692 *Bioinformatics* **47**, 11.12.1–34 (2014).
1693 92. Stitzer, M. C. *et al.* Extensive genome evolution distinguishes maize within a stable tribe of
1694 grasses. *bioRxivorg* (2025) doi:10.1101/2025.01.22.633974.
1695 93. Emms, D. M. & Kelly, S. OrthoFinder: phylogenetic orthology inference for comparative
1696 genomics. *Genome Biol.* **20**, 238 (2019).
1697 94. Rohland, N. & Reich, D. Cost-effective, high-throughput DNA sequencing libraries for
1698 multiplexed target capture. *Genome Res.* **22**, 939–946 (2012).
1699 95. Apprill, A., McNally, S., Parsons, R. & Weber, L. Minor revision to V4 region SSU rRNA
1700 806R gene primer greatly increases detection of SAR11 bacterioplankton. *Aquat. Microb.*
1701 *Ecol.* **75**, 129–137 (2015).
1702 96. Parada, A. E., Needham, D. M. & Fuhrman, J. A. Every base matters: assessing small
1703 subunit rRNA primers for marine microbiomes with mock communities, time series and
1704 global field samples. *Environ. Microbiol.* **18**, 1403–1414 (2016).
1705 97. Lundberg, D. S., Yourstone, S., Mieczkowski, P., Jones, C. D. & Dangl, J. L. Practical
1706 innovations for high-throughput amplicon sequencing. *Nat. Methods* **10**, 999–1002 (2013).
1707 98. Callahan, B. J. *et al.* DADA2: High-resolution sample inference from Illumina amplicon data.

Nat. Methods **13**, 581–583 (2016).

99. Cole, J. R. *et al.* Ribosomal Database Project: data and tools for high throughput rRNA analysis. *Nucleic Acids Res.* **42**, D633–42 (2014).

100. Bates, D., Mächler, M., Bolker, B. & Walker, S. Fitting linear mixed-effects models Usinglme4. *J. Stat. Softw.* **67**, (2015).

101. *R: A Language and Environment for Statistical Computing : Reference Index*. (2010).

102. https://CRAN.R-project.org/package=emmeans.

103. pheatmap: Pretty Heatmaps. *Comprehensive R Archive Network (CRAN)* https://CRAN.R-project.org/package=pheatmap.

104. CRAN: R News. https://CRAN.R-project.org/doc/Rnews/.

Figures

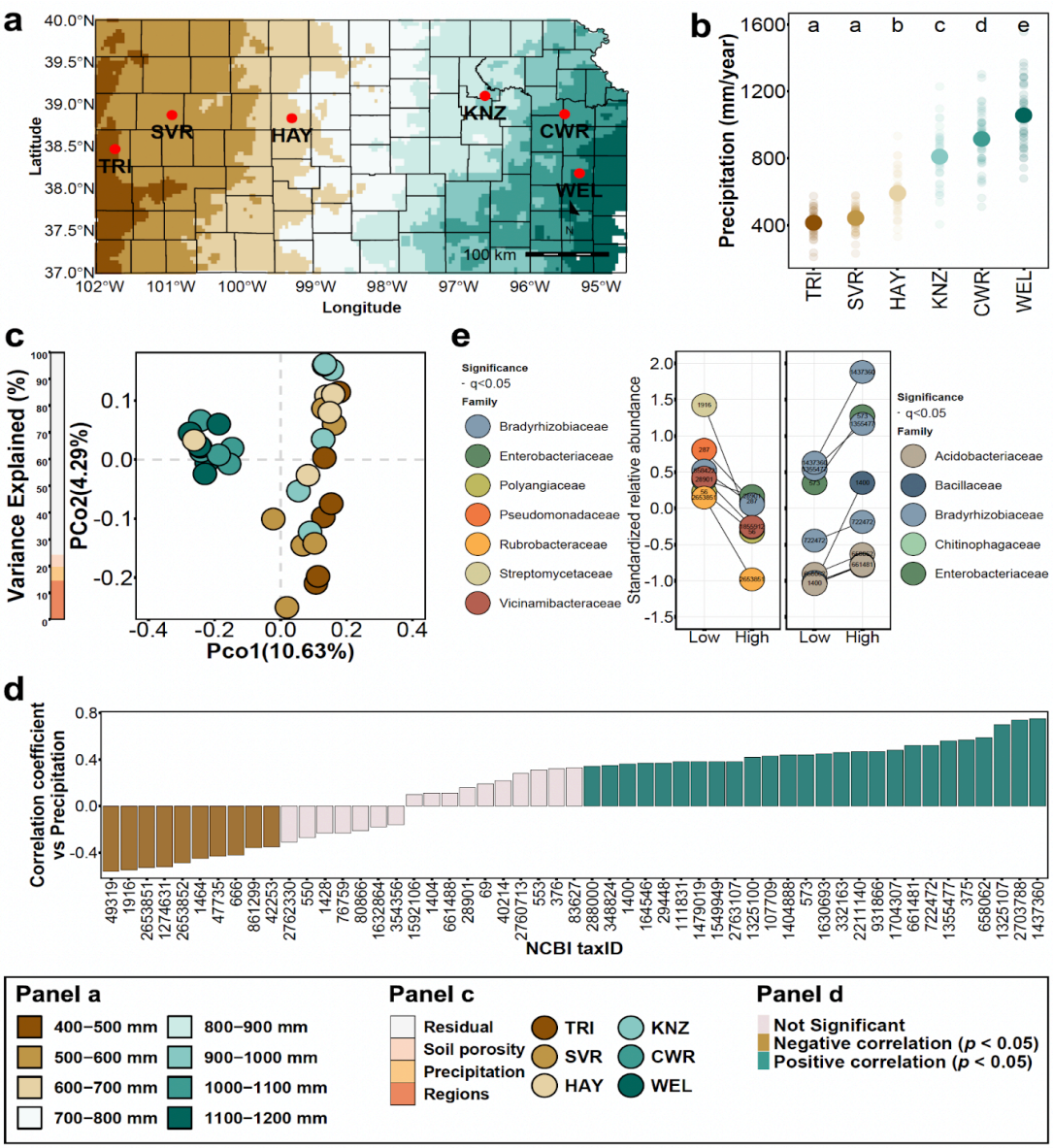

Fig. 1. Bacterial markers of precipitation after statistically controlling for other soil properties. a. Map of Kansas, USA, showing the collection locations of the soils used in this work. b. Precipitation (mm/year) at each collection site from 1981 to 2021. Large points represent the mean. Statistical difference between soils was determined via ANOVA followed by Tukey *post-hoc* test (p<0.05). c. Principal coordinate analysis of the soil microbiota across the

precipitation gradient. The bar on the left denotes the percentage of the overall variance explained by the independent variables. d. Pearson correlation coefficients between each bacterial taxon (NCBI taxID) and mean annual precipitation. e. Relative abundances of bacterial taxa identified in soils exposed to low or high precipitation levels after statistically controlling for soil porosity and mineral nutrient content. Coloured points represent the mean standardized relative abundance for each bacterial taxa. The line connecting both points is the difference between low and high precipitation soils. A black line indicates statistical significance ($q < 0.05$).

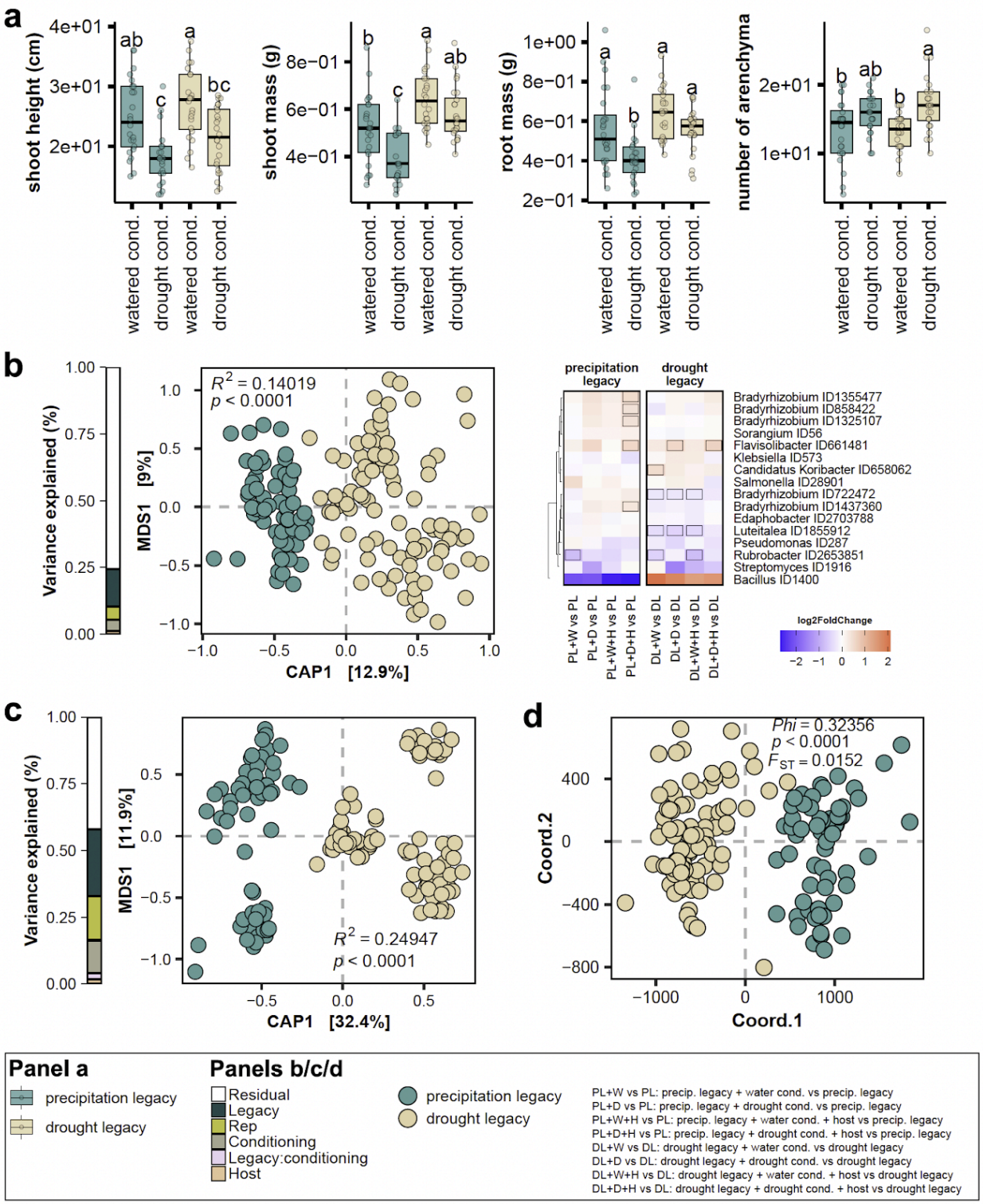

Fig. 2. Precipitation legacy effects on the soil microbiota are resilient to short-term perturbations. a. Box plots showing phenotype distributions of *Tripsacum dactyloides* plants

1736 grown during the conditioning phase, in which they experienced five months of drought (+D) or
1737 well-watered (+W) conditions and were grown in soils with either low-precipitation legacies
1738 ("DL", brown) or high-precipitation legacies ("PL", blue) (for additional phenotypes, see
1739 Extended Data Fig. 4b,d). PL and DL indicate the baseline soils prior to the initiation of
1740 conditioning phase treatments. Box edges represent the first and third quartiles; whiskers
1741 indicate the range of data points that fall within 1.5 times the interquartile range of the first and
1742 third quartiles; the center lines indicate the medians. **b.** Left: Constrained ordination of soil
1743 metagenome taxonomic composition after the conditioning phase treatments. Right: enrichment
1744 patterns of precipitation biomarker taxa in response to the different treatments, relative to the
1745 pre-conditioning baseline. Rectangles outlined in black indicate bacterial markers that were
1746 significantly enriched (red) or depleted (blue) ($q < 0.1$). **c.** Constrained ordination of soil
1747 metatranscriptome content after the conditioning phase treatments. **d.** Principal coordinates
1748 analysis of standardized pairwise genetic distances calculated from SNPs in the genomes of the
1749 precipitation biomarker taxa. For panels b-d, note that even after five months of experimental
1750 perturbation, there is a clear separation of the samples on the first axis based on the
1751 precipitation legacy.
1752

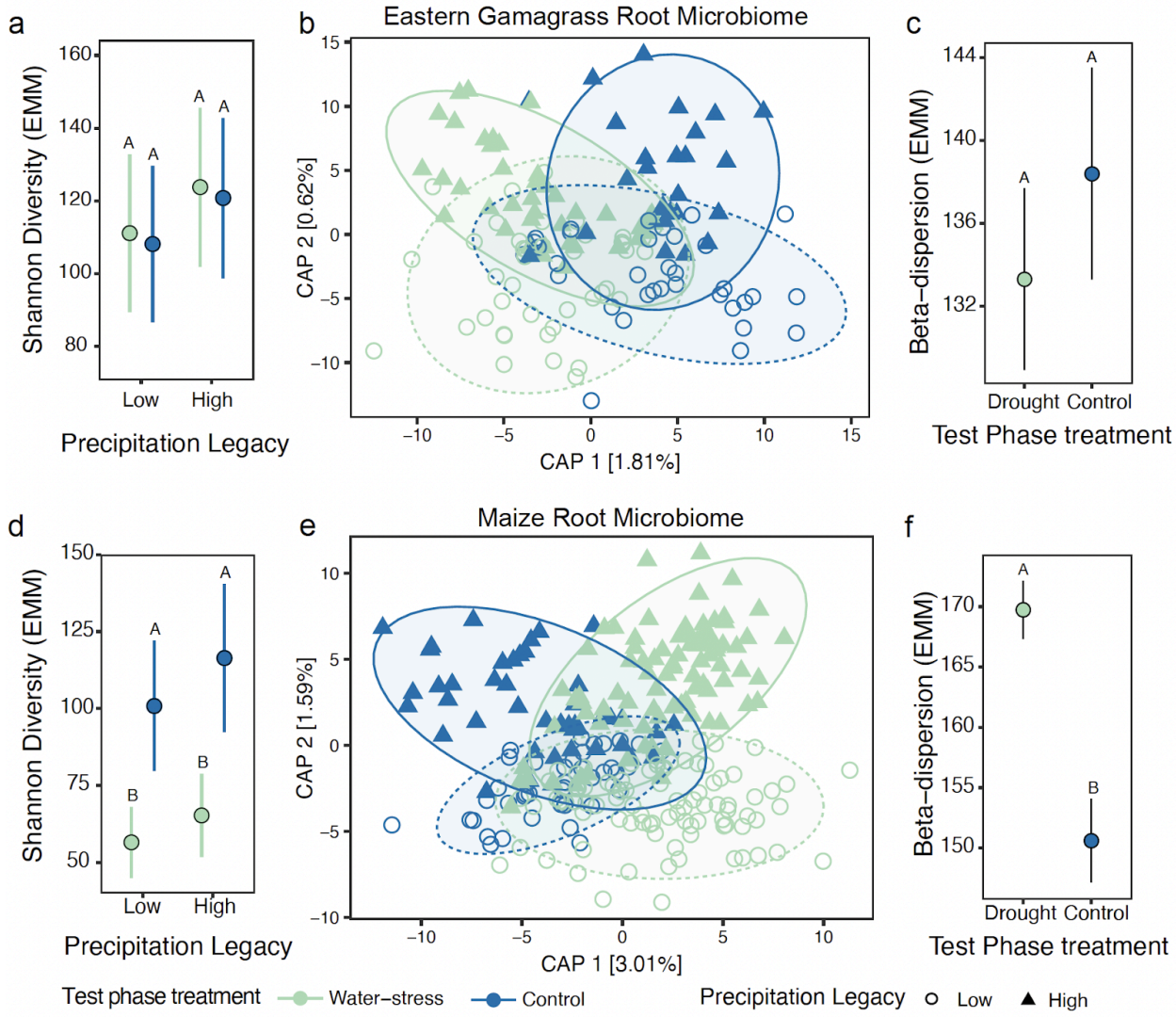

Fig. 3. Root bacterial microbiome composition is more stable in *T. dactyloides* (eastern gamagrass) than *Z. mays* (maize) plants exposed to varying inocula and water treatments. For panels a,c,d,f the points are estimated marginal means (EMMs); error bars represent standard errors; letters indicate statistical contrasts (ANOVA with Tukey's post hoc test $p<0.05$). **a.** Shannon diversity (*e*^Shannon index) was not impacted by precipitation legacy or test phase water treatment. **b**. Ordination constrained by test phase water treatment and inoculum precipitation legacy (ANOVA.CCA, full model $F_{2,139}=1.74$, $R^2=0.022$, p=0.01) indicates that test phase water treatment (ANOVA.CCA by term, $F_{1,139}=2.58$, p=0.003), but not legacy (ANOVA.CCA by term, $F_{1,139}=0.89$, p=0.55) significantly impacted the *T. dactyloides* root

1763 bacterial microbiome composition. Ellipses represent the 95% confidence intervals. **c.** Drought
1764 treatment did not impact the within-group variation (β-dispersion) of the *T. dactyloides* root
1765 microbiome. **d**. *Zea mays* (maize) root microbiome Shannon diversity was significantly impacted
1766 by test phase water treatment, but not the precipitation legacy of the inoculum. **e**. Ordination
1767 constrained by test phase water treatment and inoculum precipitation legacy (ANOVA.CCA,
1768 $F_{2,255}$=6.156, R^2=0.041, p=0.001) indicates that legacy (ANOVA.CCA by term, $F_{1,255}$=4.2538,
1769 p=0.001) and test phase water treatment (ANOVA.CCA by term, $F_{1,255}$=8.058, p=0.001)
1770 significantly impacted the *Z. mays* root bacterial microbiome composition. Ellipses represent the
1771 95% confidence intervals. **f.** Acute drought treatment increased *Z. mays* root microbiome
1772 within-group variation.
1773

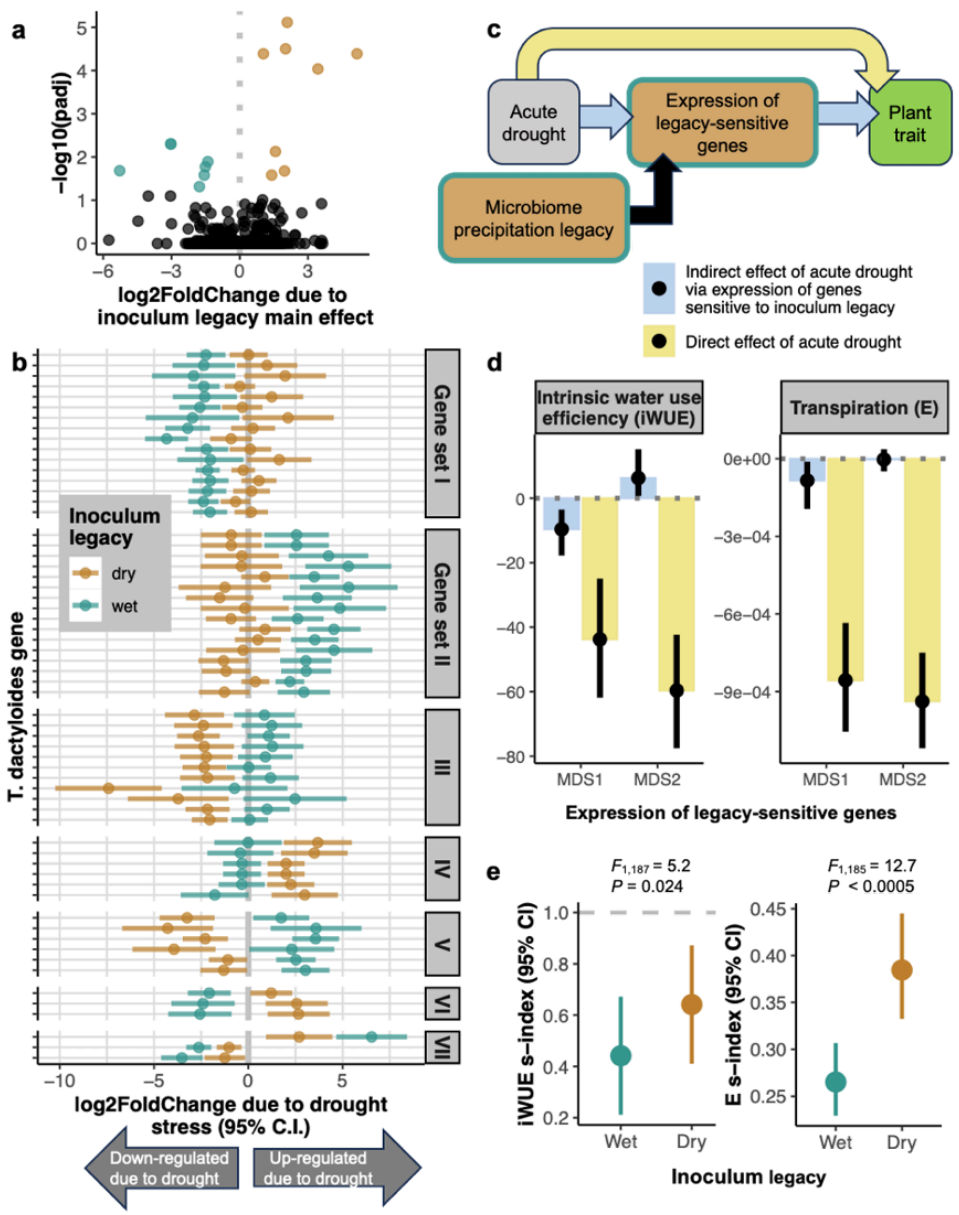

Fig. 4. The precipitation legacy of the microbial inoculum mediates transcriptional and physiological responses of *T. dactyloides* (eastern gamagrass) to acute drought. a. Fifteen genes were differentially expressed between plants inoculated with low-precipitation-legacy microbiota *vs.* high-precipitation-legacy microbiota. **b.** In total, 183 *T. dactyloides* genes responded to drought in a manner that was dependent on the drought legacy of the soil microbiota (the inoculum legacy*drought treatment interaction; Supplementary Table

1799 10). Only genes with a drought response of ≥4-fold and with annotated maize ortholog(s) are

1800 shown for illustration purposes. Each pair of points represents one gene; the position of each
1801 point illustrates how the gene's transcription level responded to drought treatment in plants
1802 inoculated with low-precipitation-legacy (brown) or high-precipitation-legacy microbiota
1803 (turquoise). Genes sets correspond to patterns of how inoculum legacy altered their drought
1804 responses. **c.** The model used for mediation analysis to test whether the expression of the 198
1805 legacy-sensitive genes (a-b) contributed to the overall effect of acute drought on plant
1806 phenotype. **d.** Mediation analysis confirmed that the expression of legacy-sensitive genes
1807 (summarized in two dimensions, MDS1 and MDS2) is involved in drought-induced decreases in
1808 intrinsic water-use efficiency (iWUE, units: μmol/mol) and transpiration (E, units: mol m^{-2} s^{-1}).
1809 Yellow bars indicate the "direct" effect of the drought treatment on trait values, i.e., the portion of
1810 the trait response that is independent of the transcription levels of microbiota legacy-sensitive
1811 genes. Blue bars show the portion of the trait response that is mediated by microbiota
1812 legacy-sensitive genes. Error bars: 95% confidence intervals. **e.** Low-precipitation-legacy
1813 microbiota (brown) stabilized iWUE and E during acute drought. The s-index describes trait
1814 values scaled by the mean value of well-watered control plants, such that an s-index of 1
1815 indicates that droughted plants were phenotypically identical to non-droughted plants. Points are
1816 EMMs and error bars indicate 95% confidence intervals.

Extended Data Figures

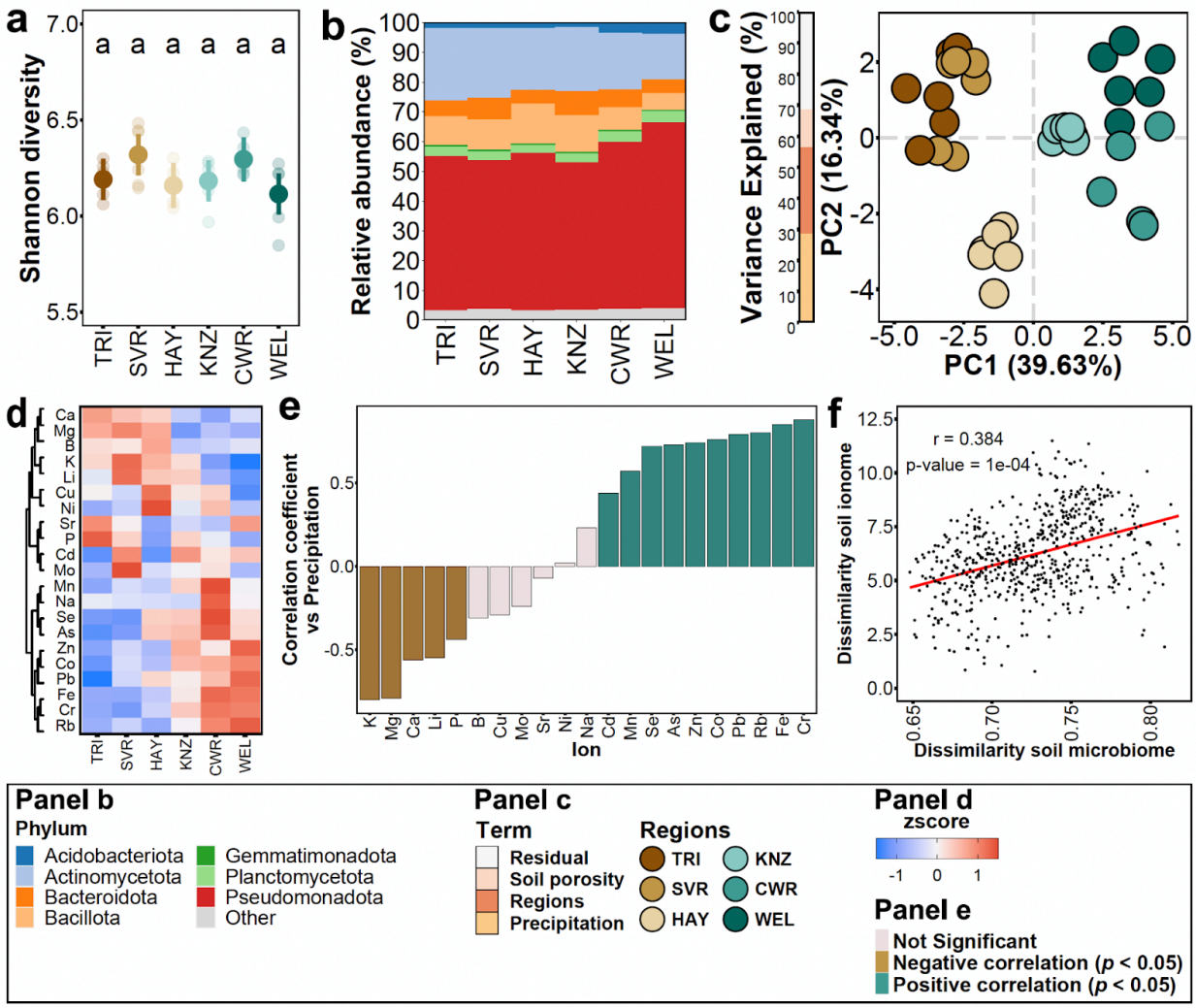

Extended Data Fig. 1. Precipitation level and mineral nutrient content in Kansas soils correlate with soil microbiota composition. a. Alpha diversity (estimated using the Shannon diversity index) did not differ across soil samples. Soils are ordered according to the gradient of precipitation (Fig 1a). **b**. Phylogram showing the relative abundance profiles of the main bacterial phyla across soils exposed to different precipitation levels. **c**. Principal component analysis showing the ionomic profiles of the six focal soils (N=6 per soil). The bar on the left denotes the percentage of the variance explained by the predictor variables. **d**. Heatmap showing the standardized concentration (z-score) of each mineral nutrient (rows) in the collection of soil exposed to different precipitation levels. The values were clustered according to the ion concentration and the region was ordered according to the precipitation gradient (low to high). **e**. Bar graph showing the Pearson correlation coefficient between each mineral nutrient abundance and the level of precipitation across the collection of soils used. Coloured bars indicate statistically significant correlations ($q < 0.05$). **f**. Pairwise correlation analysis between soil mineral nutrient dissimilarities and soil microbiome composition dissimilarities in soils representing a gradient of precipitation (N=6 per soil). Each point represents one pair of soil samples. Panel shows the Mantel test *r* statistic and its *p*-value.

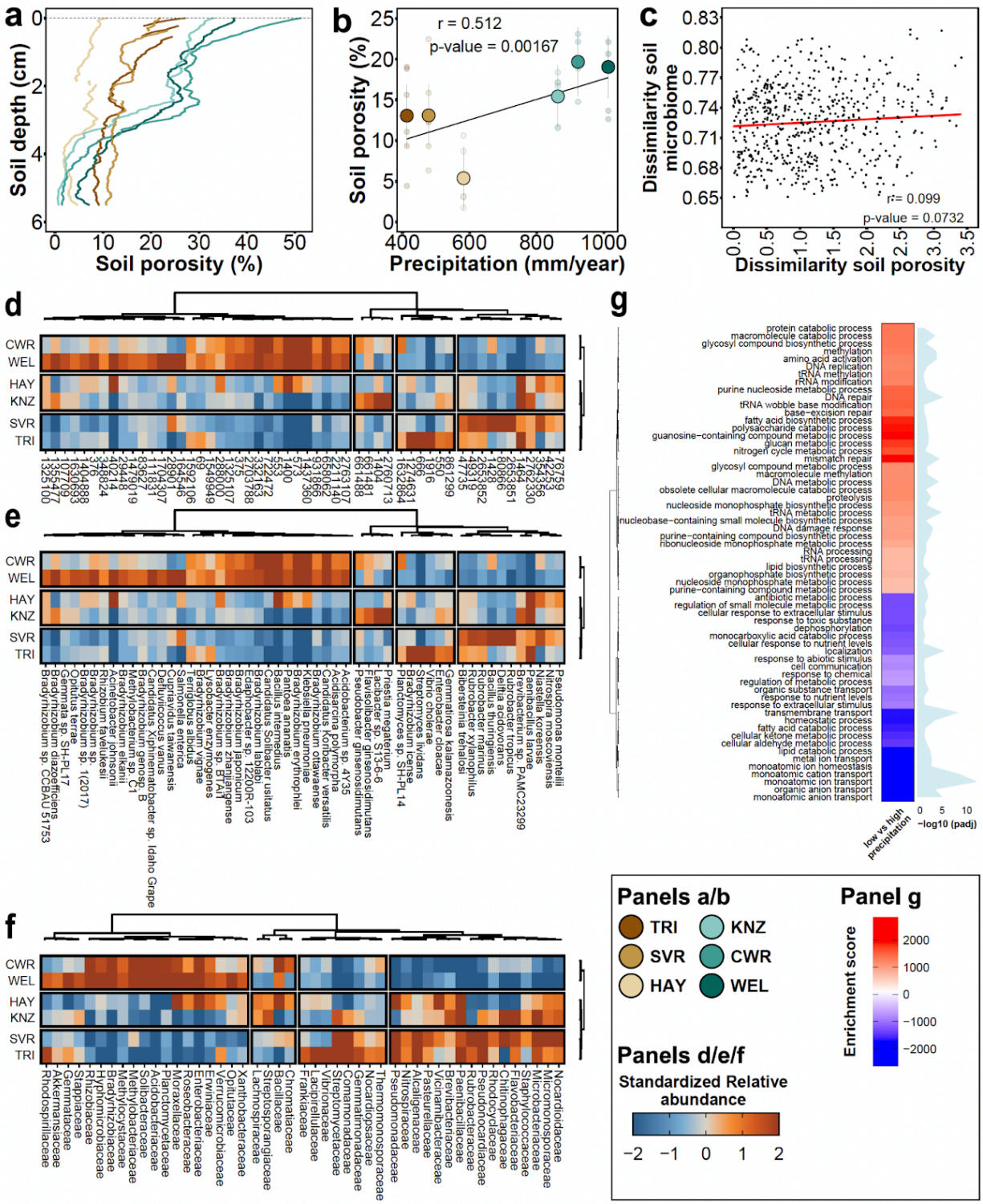

Extended Data Fig. 2. Precipitation, but not soil porosity, explains microbiota composition across the Kansas soil collection. a. Percent soil porosity changes with depth

in soils exposed to the precipitation gradient. **b**. Pearson correlation analysis between soil porosity (averaged across depths) and mean annual precipitation. **c**. Pairwise correlation analysis between soil microbiota dissimilarities and soil porosity dissimilarities. The panel shows the Mantel r statistic and its p-value. **d-f.** Heatmaps showing changes in the relative abundances of bacterial taxa (NCBI TaxIDs, **d**), species (**e**), and family (**f**) relative to the WEL soil, from the highest-precipitation site. In all cases, the values have been clustered according to taxonomic categories and soils. **g**. Numerous biological processes were enriched (red) or depleted (blue) in soils from low-precipitation sites (TRI, SVR, and HAY) relative to high-precipitation sites (WEL, CWR, and KNZ) ($q<0.05$). Gene enrichment analysis was conducted using a generalized linear model, followed by Gene Ontology (GO) classification. Enrichment scores were calculated using square root-transformed delta rank values of the GO categories.

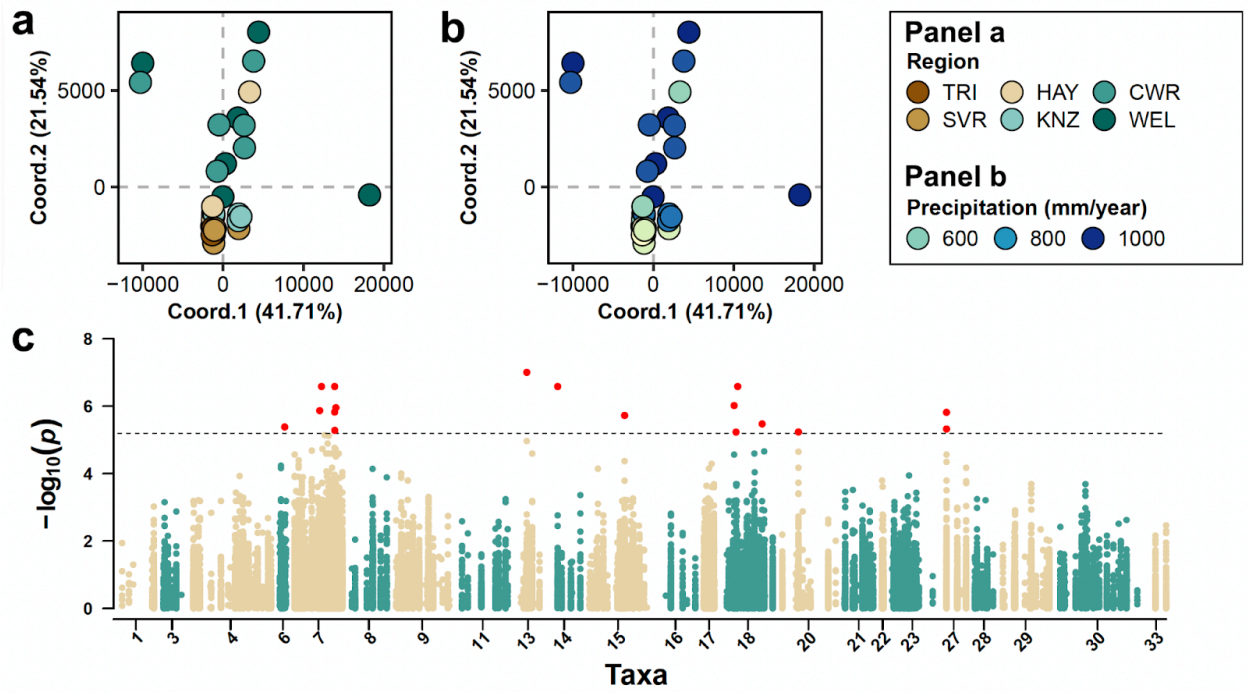

Extended Data Fig. 3. Precipitation legacy shapes the genetic differentiation of bacterial lineages within taxa. To assess genetic differences between bacterial lineages along the precipitation gradient, we selected 33 bacterial species (15 of the bacterial biomarkers of precipitation, plus 18 additional abundant and prevalent taxa) that exhibited high genome coverage in our metagenomic dataset as proxies for the broader bacterial communities. Reference genomes for each species were retrieved from the NCBI Genome database, and filtered shotgun metagenomic reads were mapped to these genomes to identify high-quality biallelic single nucleotide polymorphisms (SNPs). Genetic distances between the bacterial lineages were calculated based on the identified SNPs and PCoA plots were generated and coloured by **a**. soil collection sites and **b**. mean annual precipitation. The variance explained by each axis is indicated. **c.** The Manhattan plot illustrates significant SNPs associated with precipitation, derived from the genetic-environment association (GEA) analysis. The GEA was conducted using a general linear model, with precipitation at each sampling location as the environmental variable. Significant associations were identified using the permutation method. The x-axis of the plot represents the SNP positions along the genomes of the selected bacterial species, while the y-axis displays the -$\log_{10}$ p-values from the association model. The horizontal line indicates the statistical significance threshold, as determined by the permutation test. SNPs above this threshold, highlighted in red, were significantly associated with the precipitation gradient. Bacterial taxa with fewer than 1,000 high-quality biallelic SNPs after filtering, and with no significant SNPs detected from the GEA analysis, are not shown in the plot.

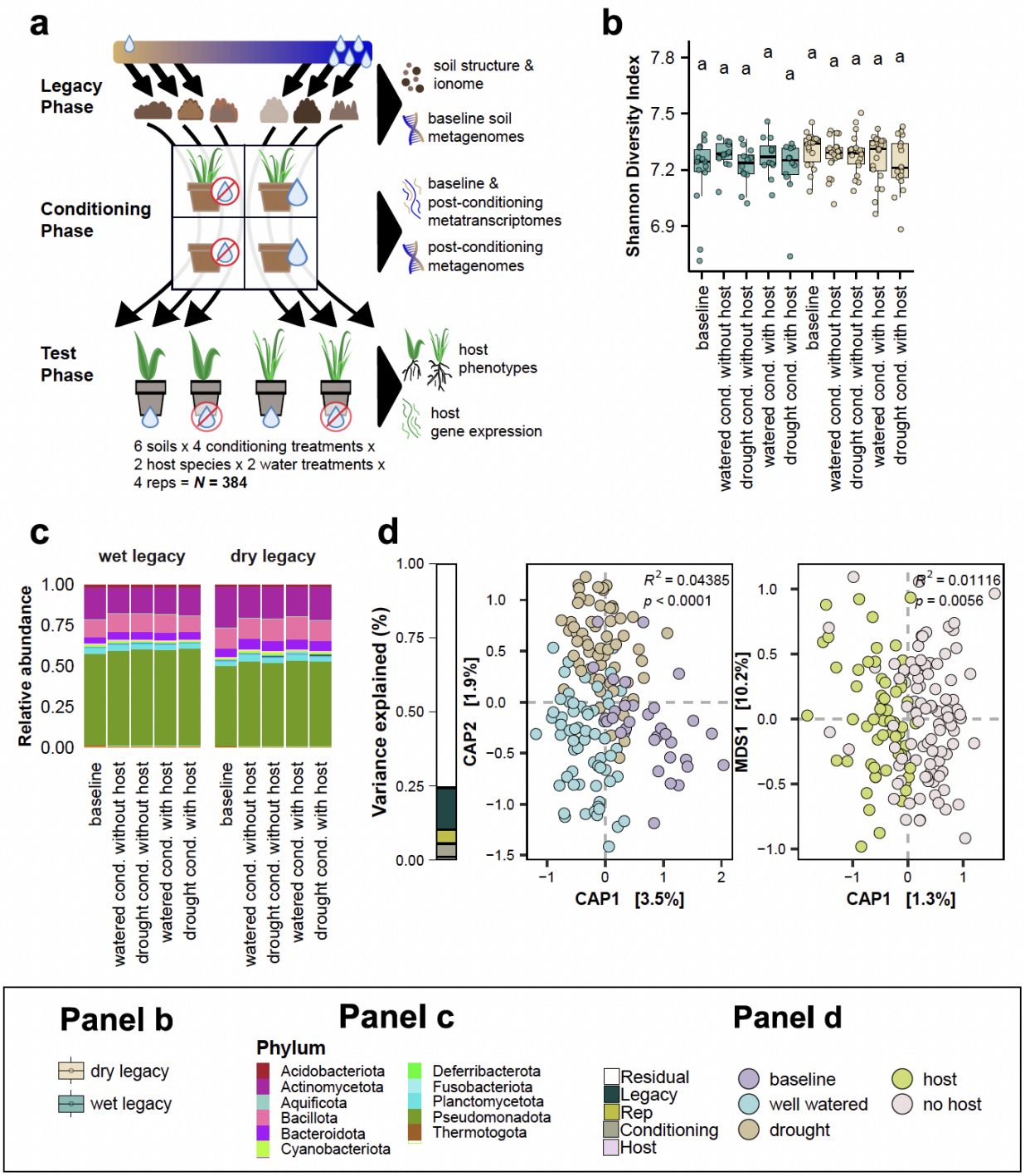

Extended Data Fig. 4. Precipitation legacy effects in the soil microbiota are resilient to short-term water- and host-related perturbations. a. Schematic representation of the experimental design used to evaluate the resilience of precipitation legacy effects to perturbations and their functional importance to plant drought response. Six soils spanning the Kansas precipitation gradient ("legacy phase"), were either left unplanted or planted with seedlings of the native grass species *Tripsacum dactyloides* (eastern gamagrass), and subjected to either drought conditions or regular watering in a factorial design ("conditioning phase"). To evaluate how soil precipitation legacy affects plants, and to disentangle the role of

the microbiota from possible effects of co-varying abiotic soil properties, we then used the experimentally-conditioned microbial communities to inoculate a new generation of *T. dactyloides* and *Z. mays* plants. These “test phase” plants were divided between water-limited conditions and well-watered control conditions. **b**. Alpha diversity of bacterial communities was not affected by the different conditioning treatments (drought or well-watered, with or without host). **c**. Phylograms show that the different conditioning treatments (drought or well-watered, with or without host) did not impact the relative abundance profiles of main bacterial phyla. **d**. Constrained ordination of metagenome taxonomic composition in response to conditioning phase treatments. Statistics are from permutational MANOVA. The bar on the left describes the percentage of the variance explained by the experimental variables.

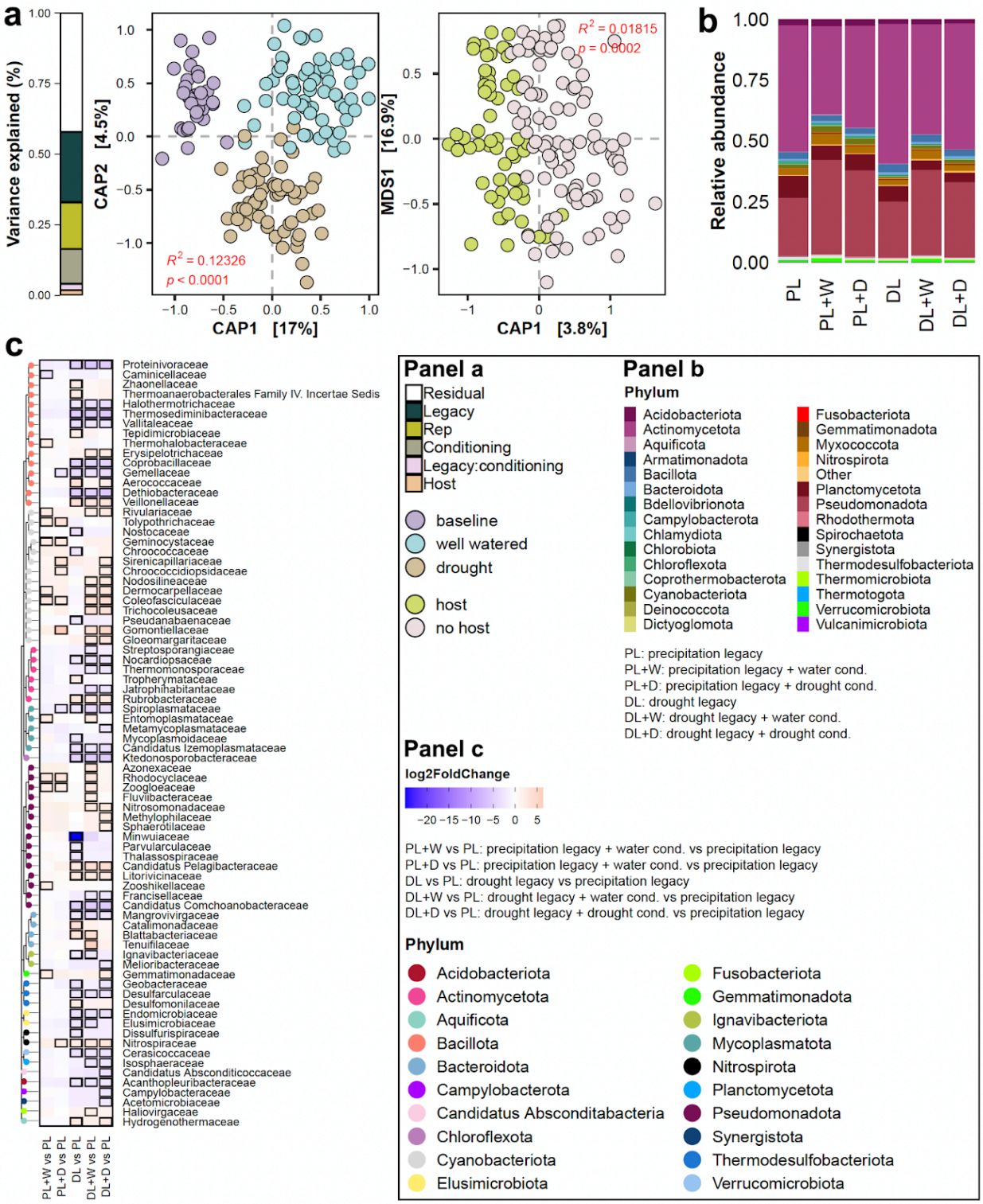

Extended Data Fig. 5. Precipitation legacy effects shape the transcriptionally-active soil microbiota even after five months of experimental perturbation. **a**. Constrained ordination of metatranscriptome content in response to conditioning phase treatments: (left) baseline soils and soils after exposure to well-watered or drought treatment, and (right) host or no-host treatment. The bar on the left describes the percentage of the variance explained by the

experimental variables. **b**. Phylogram showing the main bacterial phyla that were transcriptionally active across soils with different precipitation legacies after five months of drought or well-watered conditions, compared to the baseline for each legacy group (PL and DL). **c**. Heatmap showing enrichment or depletion of transcriptionally active bacterial families relative to the baseline high-precipitation-legacy (PL) soil. DL indicates the baseline (pre-conditioning) low-precipitation-legacy soil; +W and +D indicate five months of well-watered or drought conditions, respectively. Heatmap was coloured based on $\log_2$ fold changes derived from a generalised linear model contrasting the abundance of each family in a given treatment against the high-precipitation-legacy baseline soil. Tiles outlined in black denote statistically significant enrichment (red) or depletion (blue) ($q < 0.05$) with a $|\log_2$ fold change$| > 2$. Heatmaps were clustered based on taxonomic classification (tree on the left).

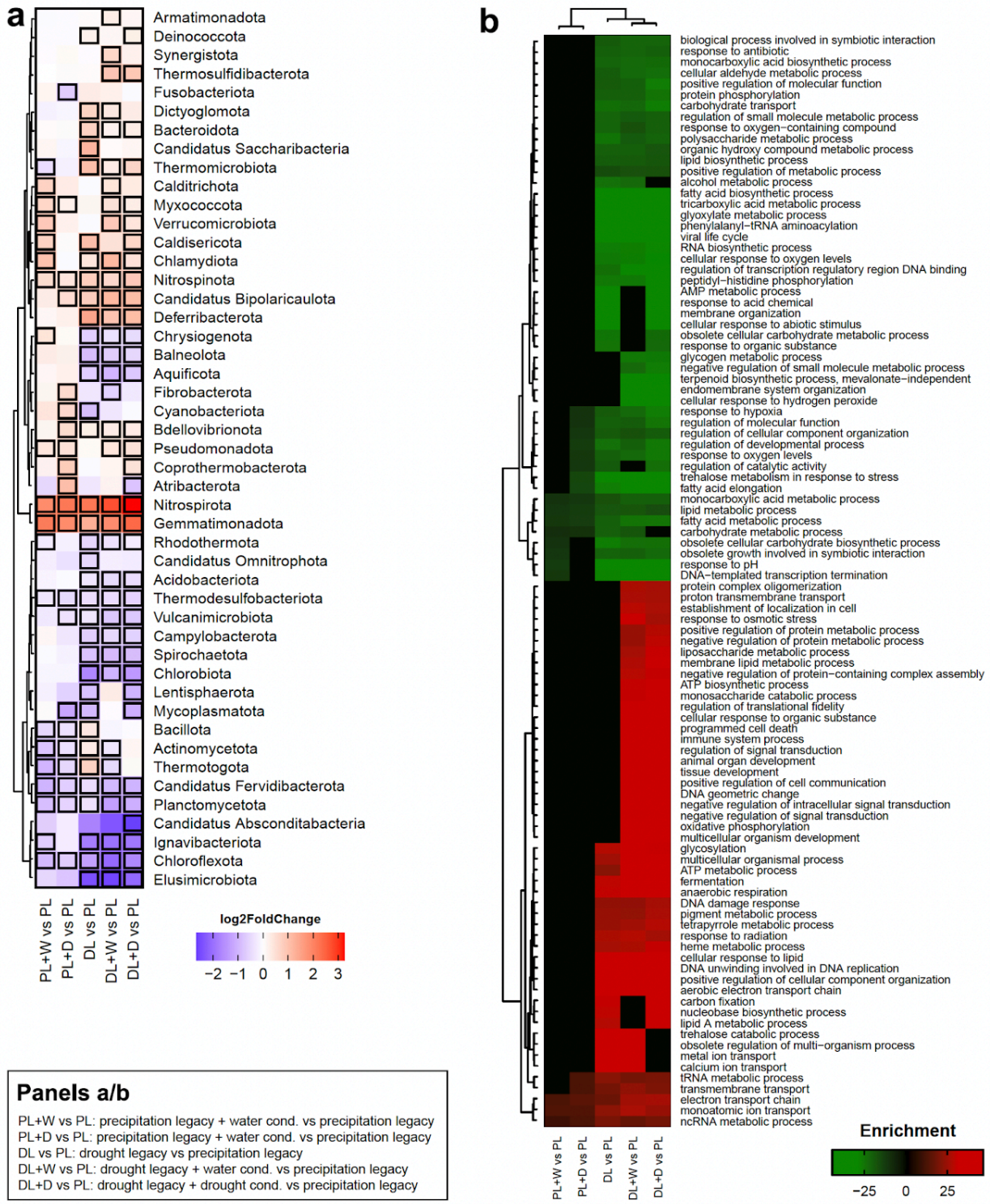

Extended Data Fig. 6. Transcriptional responses of soil microbiomes to short-term water perturbations are shaped by precipitation legacy. a. Heatmap showing the enrichment of transcriptionally active bacterial phyla in soils with low-precipitation (DL) or high-precipitation (PL) legacies, exposed to either drought (+D) or well-watered (+W) treatments, relative to the high-precipitation-legacy baseline (PL). DL indicates the baseline (pre-conditioning) low-precipitation-legacy soil. Colours represent $\log_2$ fold changes derived from a generalized

linear model comparing each treatment to the high-precipitation-legacy baseline (PL). Tiles outlined in black indicate statistically significant enrichment (red) or depletion (blue) ($q < 0.05$; $|\log_2$ fold change$| > 2$). Taxa were hierarchically clustered based on taxonomic classification (dendrogram on the left). **b**. Heatmap depicting enriched or depleted biological processes identified through metatranscriptomic analysis. Soils with high-precipitation legacies (PL) or low-precipitation legacies (DL) were subjected to five-month-long drought or well-watered treatments and then compared to the high-precipitation-legacy baseline. Gene enrichment analysis was conducted using a generalized linear model followed by Gene Ontology (GO) classification. Significantly enriched or depleted GO categories (adjusted $p < 0.05$) are coloured according to enrichment scores, calculated from square root-transformed delta rank values (red: enrichment; green: depletion). Clustering was performed based on soil treatments and GO terms.

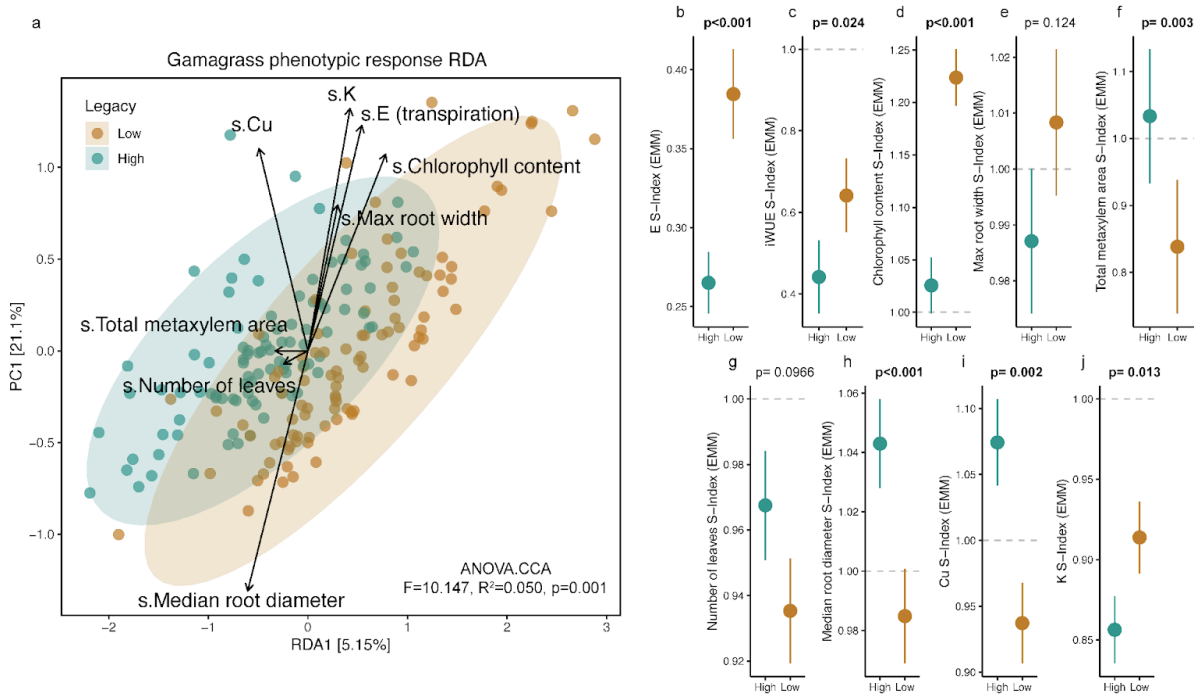

Extended Data Fig. 7. Precipitation legacy of microbial inoculum impacts gamagrass phenotypic drought response. a. A constrained redundancy analysis of the top non-collinear traits found that legacy explains 5.0% of the phenotypic response to acute drought in eastern gamagrass (*Tripsacum dactyloides*). Turquoise points represent plants that were inoculated with high-precipitation-legacy microbiota and brown points represent plants that were inoculated with low-precipitation-legacy microbiota. The ellipses indicate 95% confidence intervals. **b-j**. Assessment of individual traits indicates that microbiota with a low-precipitation legacy improved gamagrass performance under drought. Points are estimated marginal means and error bars represent the standard error, and significant p-values (≤0.05) are bolded.

a

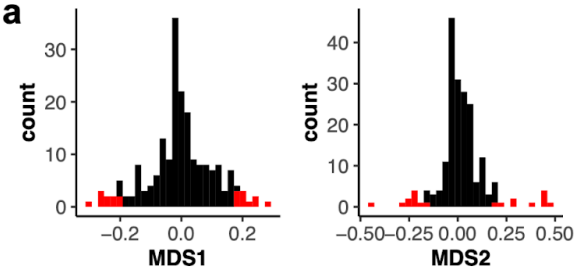

b

Number of genes		MDS1 +	MDS1 -
MDS2	+	52	54
	-	37	54

c

Top 5% of genes with strongest positive loadings on MDS1

Td_gene	MDS1	MDS2	Gene_set	Zm_orthologs	Zm_gene_symbol
Td00002ba000754	0.282	0.182	I	Zm00001eb057770	
Td00002ba018910	0.246	0.141	VII	Zm00001eb112460	cl31479_3
Td00002ba037703	0.241	-0.057	%	Zm00001eb237740	
Td00002ba002499	0.217	0.059	I	NA	
Td00002ba014047	0.21	0.021	I	Zm00001eb381580	
Td00002ba022717	0.208	0.065	III	Zm00001eb055100	
Td00002ba044330	0.205	0.103	VI	Zm00001eb199260	
Td00002ba019383	0.19	0.148	I	Zm00001eb115970	ms33
Td00002ba011993	0.181	0.078	I	Zm00001eb307550	ereb177
Td00002ba024147	0.178	0.057	I	Zm00001eb248540	umc2600a

Top 5% of genes with strongest positive loadings on MDS2

Td_gene	MDS1	MDS2	Gene_set	Zm_orthologs	Zm_gene_symbol
Td00002ba015526	-0.266	0.486	IV	Zm00001eb396120	nas7
Td00002ba015525	-0.259	0.46	IV	Zm00001eb396120	nas7
Td00002ba039891	-0.238	0.451	III	NA	
Td00002ba001144	0.168	0.447	VI	Zm00001eb053700	
Td00002ba001146	0.16	0.44	VI	Zm00001eb053700	
Td00002ba041411	-0.173	0.389	IV	NA	
Td00002ba015516	-0.141	0.272	IV	Zm00001eb396120	nas7
Td00002ba015515	-0.141	0.272	IV	Zm00001eb396120	nas7
Td00002ba033830	-0.15	0.218	V	Zm00001eb039280	ga20ox7
Td00002ba019393	-0.154	0.199	III	Zm00001eb286420	mads58

Top 5% of genes with strongest negative loadings on MDS1

Td_gene	MDS1	MDS2	Gene_set	Zm_orthologs	Zm_gene_symbol
Td00002ba046162	-0.203	0.116	V	Zm00001eb199320	
Td00002ba046161	-0.206	0.112	II	Zm00001eb199320	
Td00002ba036367	-0.222	0.138	II	Zm00001eb199320	
Td00002ba036368	-0.224	0.132	II	Zm00001eb199320	
Td00002ba019546	-0.236	-0.222	II	Zm00001eb147080	
Td00002ba039891	-0.238	0.451	III	NA	
Td00002ba007195	-0.257	0.113	II	Zm00001eb161990	
Td00002ba015525	-0.259	0.46	IV	Zm00001eb396120	nas7
Td00002ba015526	-0.266	0.486	IV	Zm00001eb396120	nas7
Td00002ba002239	-0.304	0.188	III	Zm00001eb048620	

% downregulated due to main effect of dry-legacy inoculum (no interaction with drought)

Top 5% of genes with strongest negative loadings on MDS2

Td_gene	MDS1	MDS2	Gene_set	Zm_orthologs	Zm_gene_symbol
Td00002ba023452	-0.061	-0.166	V	Zm00001eb027750	pat3
Td00002ba021901	0.012	-0.19	V	NA	
Td00002ba019546	-0.236	-0.222	II	Zm00001eb147080	
Td00002ba019177	0.023	-0.222	III	Zm00001eb180130	
Td00002ba009640	-0.077	-0.222	II	Zm00001eb210740	AY110625
Td00002ba008826	-0.138	-0.224	II	Zm00001eb125560	umc1742
Td00002ba045645	-0.019	-0.24	*	NA	
Td00002ba015343	0.124	-0.267	II	NA	
Td00002ba006731	-0.084	-0.272	II	Zm00001eb210740	AY110625
Td00002ba006546	-0.029	-0.435	VIII	Zm00001eb211300, Zm00001eb211310, Zm00001eb155430, Zm00001eb055690	pco095801, AY106518, GRMZM2G024958

* upregulated due to main effect of dry-legacy inoculum (no interaction with acute drought)

Extended Data Fig. 8. Expression patterns of *Tripsacum dactyloides* genes in relation to microbiome legacy and NMDS axes that mediate drought responses. **a**. Histograms showing the distributions of gene loadings onto both axes of an ordination based on non-metric multidimensional scaling of RNA-seq data (see Fig. 4). The top 5% of genes with the strongest positive and negative loadings onto each axis are in red. **b**. Breakdown of the number of genes with positive/negative loadings onto each axis. **c**. Lists of genes comprising the 5% tails of the distributions in panel (a). Detailed information about the expression responses of these genes is available in Supplementary Table S10. 'Gene_set' refers to the patterns of response to microbiome legacy presented in Fig. 4a-b.

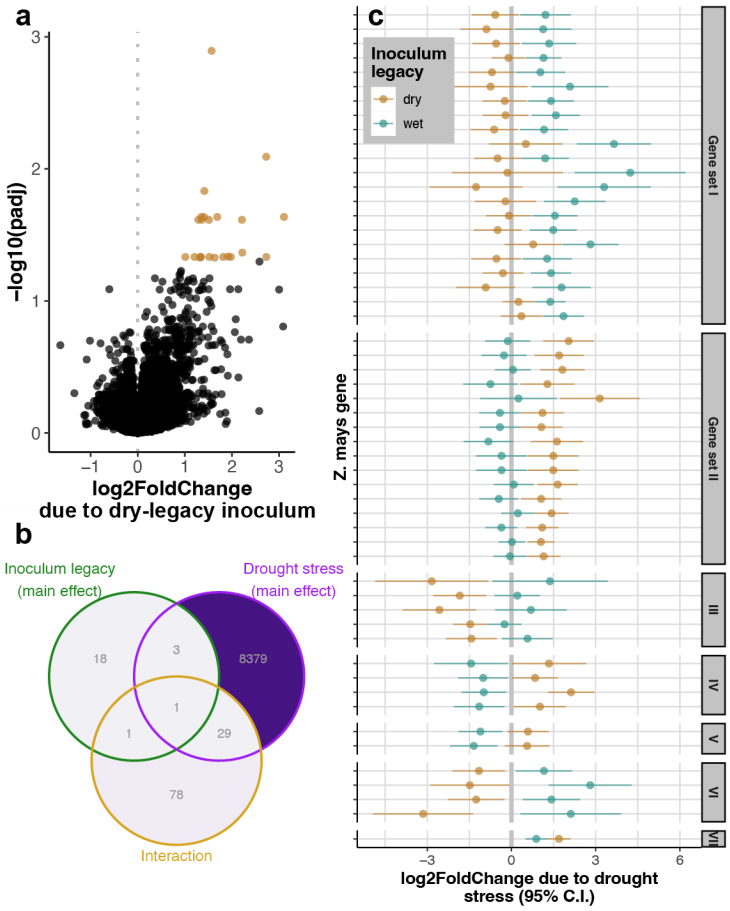

Extended Data Fig. 9. Precipitation legacy of microbial inocula alters the transcriptional response to drought in the maize crown root. a. 23 genes were up-regulated in plants inoculated with soil microbiota from a low-precipitation region, relative to plants inoculated with microbiota from a high-precipitation region. **b.** The sets of genes that responded to the main effects of inoculum legacy and test phase drought treatment had little overlap with each other or with the set of genes that were sensitive to the interaction between the two. **c.** In total, 109 maize genes responded to drought in a manner that was dependent on the drought legacy of the soil microbiota (the inoculum legacy * drought treatment interaction term), regardless of the inoculum's treatment during the conditioning phase. For illustration purposes, only annotated genes with $|\log_2\text{FoldChange}| > 1$ in at least one microbial context are shown here; the full list is available in Supplementary Table S10. Each pair of points shows one gene; the position of each point illustrates how the gene's expression changed in response to drought stress during the Test Phase, depending on whether the plant had been inoculated with microbiota derived from a low-precipitation (brown) or dry-precipitation (turquoise) environment. Genes are grouped into sets according to the pattern of how inoculum legacy altered their drought responses. Note: the names of these gene sets are not meant to correspond to the names of the *T. dactyloides* gene sets shown in Fig. 4b; in each species, Gene set I contains the most genes, Gene set II contains the next most, and so on.

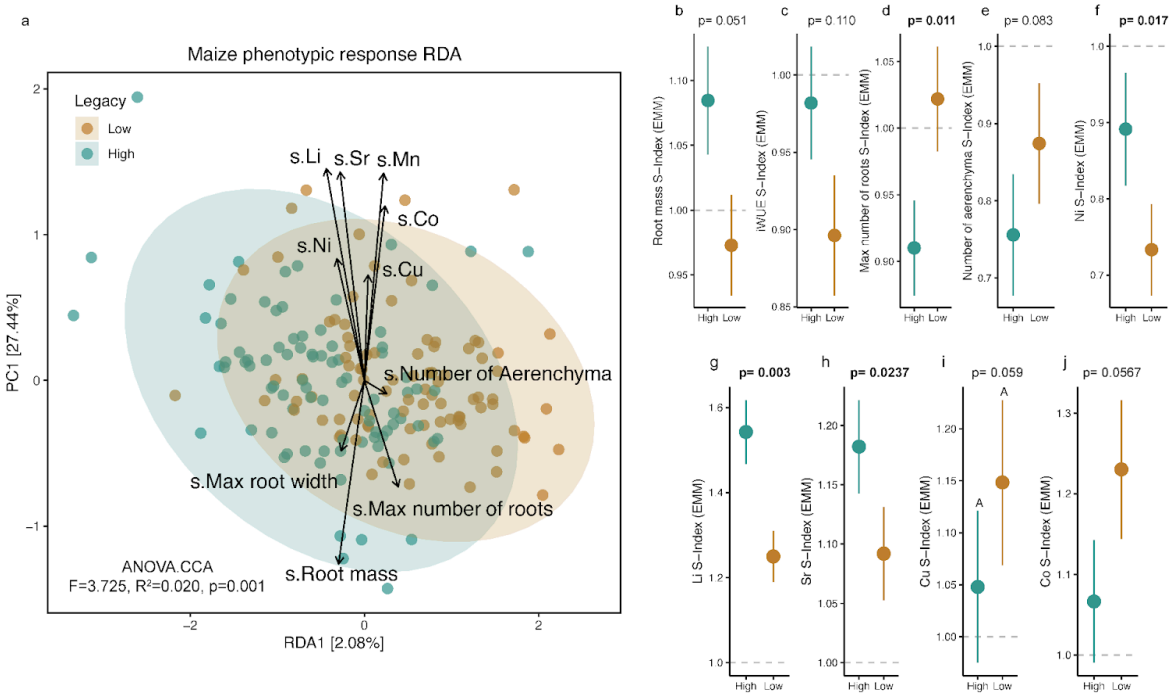

Extended Data Fig. 10. Precipitation legacy of the microbiota had only weak impacts on the phenotypic drought response of maize, compared to that of eastern gamagrass. For comparison, the effects of microbiota precipitation legacy on eastern gamagrass drought responses are shown in Fig. 4 and Extended Data Fig. 7. **a.** A constrained redundancy analysis of the top non-collinear traits found that the precipitation legacy of the microbial inoculum only explains 2.0% of the maize phenotypic response to acute drought. Turquoise points represent root microbiomes with high precipitation legacy and brown points represent those with low precipitation legacy. The ellipses indicate 95% confidence intervals. **b-j.** Assessment of individual traits indicates that microbiota with a low-precipitation legacy did not significantly improve maize performance under drought, but did impact several mineral nutrient concentrations. Points are estimated marginal means and error bars represent the standard error, and significant *p*-values (≤ 0.05) are bolded.